nature materials

LETTERS

https://doi.org/10.1038/s41563-020-00803-5

Recapitulating macro-scale tissue self-organization through organoid bioprinting

Jonathan A. Brassard[1,3], Mike Nikolaev[1,3], Tania Hübscher[1,3], Moritz Hofer[1] and Matthias P. Lutolf[1,2]✉

Bioprinting promises enormous control over the spatial deposition of cells in three dimensions[1–7], but current approaches have had limited success at reproducing the intricate micro-architecture, cell-type diversity and function of native tissues formed through cellular self-organization. We introduce a three-dimensional bioprinting concept that uses organoid-forming stem cells as building blocks that can be deposited directly into extracellular matrices conducive to spontaneous self-organization. By controlling the geometry and cellular density, we generated centimetre-scale tissues that comprise self-organized features such as lumens, branched vasculature and tubular intestinal epithelia with in vivo-like crypts and villus domains. Supporting cells were deposited to modulate morphogenesis in space and time, and different epithelial cells were printed sequentially to mimic the organ boundaries present in the gastrointestinal tract. We thus show how biofabrication and organoid technology can be merged to control tissue self-organization from millimetre to centimetre scales, opening new avenues for drug discovery, diagnostics and regenerative medicine.

Bioprinting has been widely applied in tissue engineering and regenerative medicine due to its powerful ability to control large-scale depositions of cells and biocompatible materials[1]. Although robust bioprinting modalities such as multimaterial[2], in situ[3], freeform[4–7] and smart material bioprinting[8,9] have recently been developed, these methods compromise the suitability of the cellular environment to improve printability and resolution. This tradeoff has precluded the high cellular density and permissiveness necessary to recreate the complexity of native tissue architecture and function.

In vivo, tissue formation relies heavily on a tightly regulated morphogenetic program that allows groups of cells to locally interact and self-organize. Iterative interactions between these locally developing tissue units guide successive cycles of cellular differentiation and patterning that establish biological complexity over a large scale. Because of their unique self-organization potential, stem cell-derived organoids are promising tissue mimetics that are unmatched by engineering methods in terms of reproducing local features of tissue architecture and cell-type composition[10,11]. However, because organoids cannot be grown beyond the millimetre scale, they lack architectural features of native organs that would allow the emergence of higher-level functional characteristics[12,13]. An important step towards in vitro tissue and organ development for regenerative medicine involves controlling the self-organization potential of mammalian cells at the macroscopic scale, but this remains challenging with existing technologies. A better control over tissue size and architecture could ultimately provide artificial organs to be used for drug screening or eventual organ replacements, lessening the burden on animal testing and removing the long wait times for transplants.

Here we introduce a three-dimensional (3D) bioprinting concept for guiding tissue morphogenesis across more physiologically relevant scales and directly within highly permissive extracellular matrices (ECMs) that facilitate effective multicellular self-organization. Our approach, termed bioprinting-assisted tissue emergence (BATE), uses stem cells and organoids as spontaneously self-organizing building blocks that can be spatially arranged to form interconnected and evolving cellular constructs (Fig. 1a). Hence, each cell or cellular aggregate that would normally develop into a relatively randomly shaped small organoid can be coerced to fuse and reorganize, following the geometry and constraints imposed by 3D printing. Using this versatile strategy, large-scale cellular constructs can be printed with key cell types—for example, parenchyma and its corresponding stroma, or different epithelial cells from the gastrointestinal tract—in an effort to reproduce the tissue–tissue interactions seen in native organ development or in homeostasis.

One critical challenge in bioprinting is to screen for the optimal combination of nozzle diameter, extrusion pressure and printhead speed required depending on the bioink composition, rheological properties and cellular concentration. To solve this costly optimization, we designed an easy-to-build and broadly applicable printing set-up consisting of a syringe-based extrusion system coupled to a microscope with a manually controlled stage (Fig. 1a and Extended Data Fig. 1a). Microscope-based bioprinting lowers the need for in-depth expertise on hydrogel rheology and bioink formulation as it facilitates printout optimization by providing direct user feedback for visually controlling and modulating the printing process in real time. Cells can be sequentially aspirated and accurately deposited directly inside liquid precursors of typical ECM hydrogels during their gelation (Supplementary Video 1). By adjusting the nozzle size (50–200 μm), flow rate (5–200 nl s^{-1}) and printing speed (defined by the microscope stage handling), we can control the final cellular density, down to lines of single cells if desired (Fig. 1b and Extended Data Fig. 1b–d). Printing of relatively complex designs, such as discontinuous patterns with various cell densities, can be facilitated by using a programmed dispensing of the syringe.

Due to their favourable viscosity range, a wide variety of commonly used cell and organoid culture matrices such as Matrigel, collagen I or methylcellulose are compatible with BATE, in some

[1]Laboratory of Stem Cell Bioengineering, Institute of Bioengineering, School of Life Sciences and School of Engineering, Ecole Polytechnique Fédérale de Lausanne (EPFL), Lausanne, Switzerland. [2]Institute of Chemical Sciences and Engineering, School of Basic Science (SB), EPFL, Lausanne, Switzerland. [3]These authors contributed equally: Jonathan A. Brassard, Mike Nikolaev, Tania Hübscher. ✉e-mail: matthias.lutolf@epfl.ch

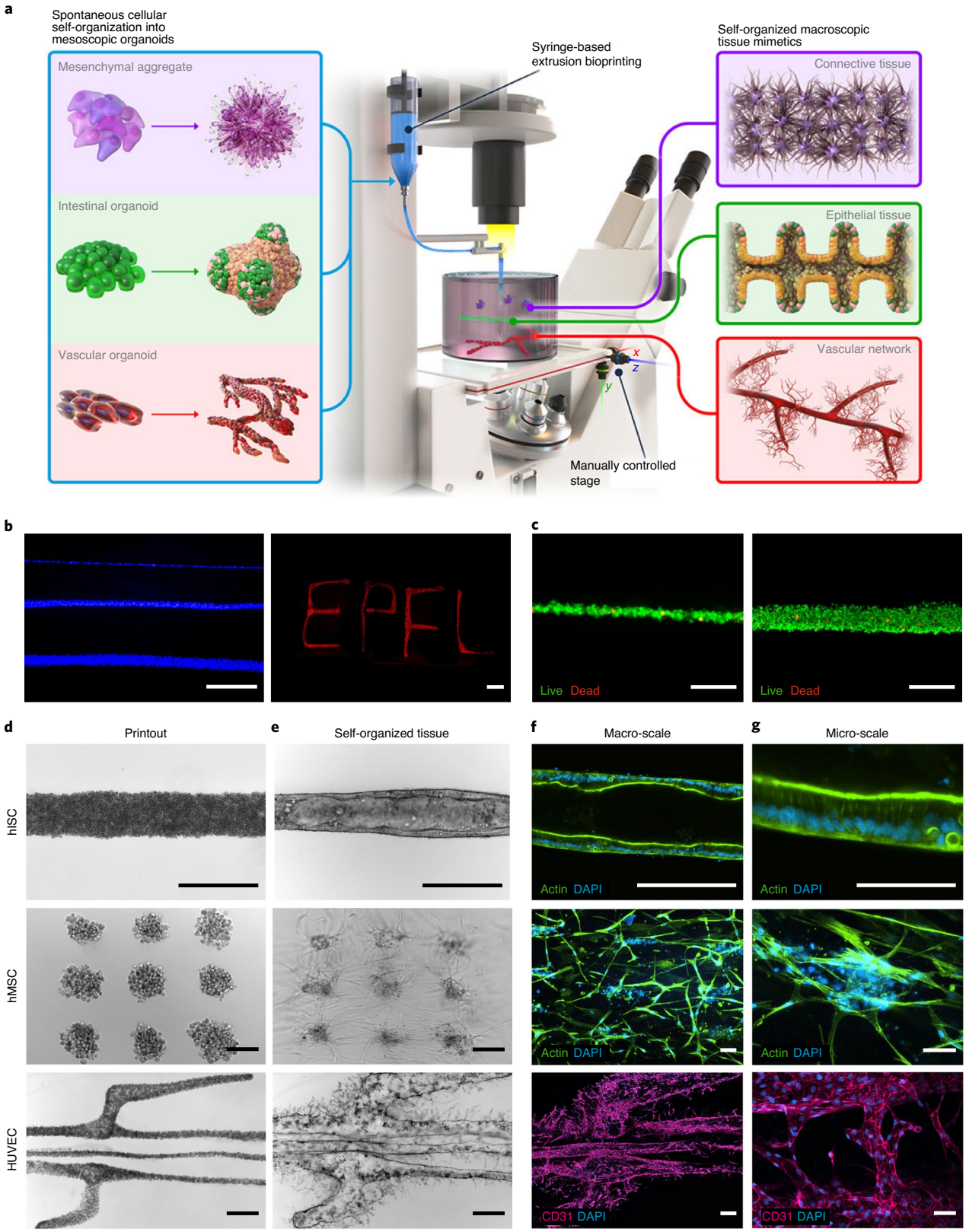

Fig. 1 | BATE. a, Illustration of the BATE concept using spontaneously self-organizing building blocks to create large-scale tissues. **b**, Representative fluorescent images of cells stained with cell tracker dyes showing the modulation of the resolution (left) and printing of complex geometry (right). Scale bars, 500 µm. **c**, Representative images of viability of HUVECs after printing with a low (left) and high (right) density, shown by calcein AM (live, green) and ethidium homodimer-1 (dead, red) cell stainings. See also Extended Data Fig. 1e for quantification. Scale bars, 250 µm. **d**,**e**, Bright-field images of the cell patterning immediately after printing (**d**) and after self-organization (**e**) of hMSC, hISC and HUVEC cells. Scale bars, 500 µm. **f**,**g**, Fluorescence confocal images of macroscopic (**f**) and microscopic (**g**) tissue architecture. Cells are labelled with DAPI (blue) and F-actin (green) or CD31 (pink). All images are representative of $n = 3$ biologically independent experiments. Scale bars, 250 µm (**f**) and 75 µm (**g**).

cases requiring an optimization of the temperature and bio-ink concentration to achieve good printing fidelity. The use of these cell-instructive matrices allows high-density cell suspensions (up to 100 million cells per ml) to be readily available as bioink for 3D printing without compromising cellular viability (Fig. 1c and Extended Data Fig. 1e) and cell-intrinsic self-organization (Fig. 1d–g).

To illustrate the potential and flexibility of our approach for guiding the macro-scale self-organization of primary cells derived from human tissues, we printed three cell types with known self-organizing (or self-assembling) potentials that originated from tissues that play critical roles during organ morphogenesis and function; namely, epithelial, connective and vascular tissues (Fig. 1d–g). Over the course of several days, human intestinal stem cells (hISCs) printed in a line (here, 5–15 mm in length) inside a viscous Matrigel/collagen precursor solution morphed into a connected and polarized epithelial tube in the crosslinked matrix (Fig. 1d–g), recapitulating the tissue organization found in classical hISC-derived organoids[14]. The establishment of intestinal epithelial tubes was found to be highly dependent on the ECM type and culture conditions (Extended Data Fig. 2), highlighting the importance of the more bioactive ECM support and media in cellular remodelling and morphogenesis after bioprinting. Similar results were obtained with primary mouse colon and stomach stem cell, as well as with human colon stem cells (Extended Data Fig. 3), indicating that BATE may be broadly applicable to epithelial stem cell-derived organoids.

Human mesenchymal stem/progenitor cells (hMSCs) precisely positioned in a 3D Matrigel and collagen mixture readily migrated and invaded the surrounding ECM, establishing a fibrous connective tissue-like structure (Fig. 1d–g). Furthermore, by 3D printing human umbilical vein endothelial cells (HUVECs), we also formed self-organized branched vascular tubes with a lumen that can be perfused (Fig. 1d–g and Extended Data Fig. 4). When printed in collagen I and stimulated with a high concentration of vascular endothelial growth factor (VEGF), the HUVECs formed de novo capillaries[15] (Fig. 1d–g, Extended Data Fig. 5 and Supplementary Video 2). By timing the exposure to VEGF, angiogenesis was robustly triggered at the tissue scale, resulting in an interconnected vascular network and tubes featuring continuous lumen. Notably, in defective printouts, for example caused by cell aggregation during printing, the multicellular self-organization resulted in the smoothening of small defects or variations while maintaining the prescribed macroscopic geometry (Extended Data Fig. 5). These experiments show that the specific local interactions that control self-organization of a small cellular unit can be multiplied and systematically arranged to form epithelial tubes, connective tissues and vascular networks with a defined geometry.

Next, we attempted to reconstruct an intricately patterned tissue at the macro-scale, which required the precise manipulation of geometry, cell–cell interactions, ECM composition and dynamics and the presence of key soluble factors (Fig. 2a). Mouse intestinal stem cells (mISCs), when cultured in Matrigel and supplemented with a defined cocktail of growth factors (EGF, Noggin and R-spondin (ENR)), form organoids bearing crypts and villus-like compartments resembling the epithelium of the small intestine in vivo[16,17]. Dense lines of 3D-printed mISCs, cultured in ENR, developed into epithelial tubes in Matrigel as well as stiffer Matrigel and collagen mixtures (Extended Data Fig. 6 and Supplementary Videos 3 and 4). Guided by the imposed cylindrical geometry, bioprinted ISCs first condense into a thick tubular construct lacking a lumen before expanding as colonies and then fusing soon after into a polarized and lumenized epithelial tissue (Fig. 2b, Supplementary Video 3 and Extended Data Fig. 7). After 4–6 days, the epithelial tubes bud (Fig. 2b) in a process that appears to coincide with the emergence of individual Paneth cells, which are distinguishable by their characteristic morphology and darker appearance, interspersed with stem cells expressing the characteristic marker Lgr5 (Extended Data Fig. 7). This finely spaced salt and pepper-like cellular arrangement is reminiscent of the patterning of Paneth cells and stem cells in the intestinal crypts in vivo and in organoids[16,17]. Even though dead cells are shed inside the epithelium as in classical organoids, intestinal tubes can be cultured for longer periods (≥3 weeks) and reach a larger diameter (>400 μm) (Fig. 2c,d). During this remodelling process, the length of the tube increases only slightly (less than 10% in 3 weeks), demonstrating that the increase in diameter is due to proliferation and growth.

A critical parameter for colony fusion is a very high density of cells, probably because confined colony growth exerts compressive forces and increases colony-colony contact, subsequently promoting fusion. Indeed, although small organoids can also be used for printing, the resulting tubes are often discontinuous and show relatively high variation in their diameter, mainly due to irregular organoid fusion in the absence of the condensation step seen with single-cell printing (Extended Data Fig. 8). Furthermore, tubes printed at lower density (12.5 million cells per ml) not only have a smaller diameter (Fig. 2e), but also suffer from decreased robustness and reproducibility, as exemplified by some discontinuities as well as a heterogeneous distribution of their crypts (Extended Data Fig. 8). Using high single-cell density (≥50 million cells per ml), the printed tubes are highly reproducible, each of them having a comparable diameter (Fig. 2e) and featuring a continuous lumen as shown by histological analysis (Fig. 2f). Following matrix degradation, epithelial tubes can then be released and manually handled, indicating a surprising mechanical resiliency (Fig. 2g). Together, these data demonstrate that by spatially arranging spontaneously self-organizing tissue building blocks in permissive ECMs, complex tissue architecture and patterning can be robustly reproduced at the centimetre scale.

To characterize the cellular composition of the printed intestinal tissues, eight-day-old tubes were stained to reveal putative crypts (marked by Sox9) with Paneth cells (Lyz), as well as a villus-like domain positive for the enterocyte marker L-FABP (Fig. 3a–c). Proliferative cells, labelled by the thymidine analogue 5-ethynyl-2'-deoxyuridine (EdU), were exclusively found in crypts (Fig. 3d). Transmission electron microscopy demonstrated the presence of mature differentiated cell types in the tubes, such as enterocytes with a characteristic apical brush border, mucus-producing goblet cells and enteroendocrine cells (Fig. 3e–g). Histological analysis using Alcian Blue showed goblet cells and a mucus layer covering the apical side of the epithelium (Fig. 3h).

Next, we assessed the physiological responses of the intestinal tubes to chemical stimuli. Paneth cells are a chief player in innate mucosal immunity and contain large apical secretory granules rich in host defence peptides such as lysozyme and defensins. To assess this secretory response, we used a lysozyme reporter organoid line (Lys-dsRED mISCs)[18]. Cells were printed and cultured for 6 days before being exposed basally to 100 μM carbamylcholine to trigger release of lysozyme granules from Paneth cells[19] (Fig. 3i). On chemical treatment, the tubes immediately responded by swelling, followed by liberation of the lysozyme granules in their lumen (Supplementary Video 5). Additionally, we characterized the ability of the intestinal tubes to swell in response to the activation of the cystic fibrosis transmembrane conductance regulator channels[20]. Eight-day-old intestinal tubes exposed to 20 μM forskolin rapidly swelled, showing expansion of their diameter by more than 20% after 1 h (Fig. 3j,k and Supplementary Video 5). These results show that BATE can yield engineered tissues with high physiological relevance, resembling the phenotype and functionalities of their in vivo counterparts.

In the embryo and adult organism, different organ tissues continuously interact to provide precise spatiotemporal cues that

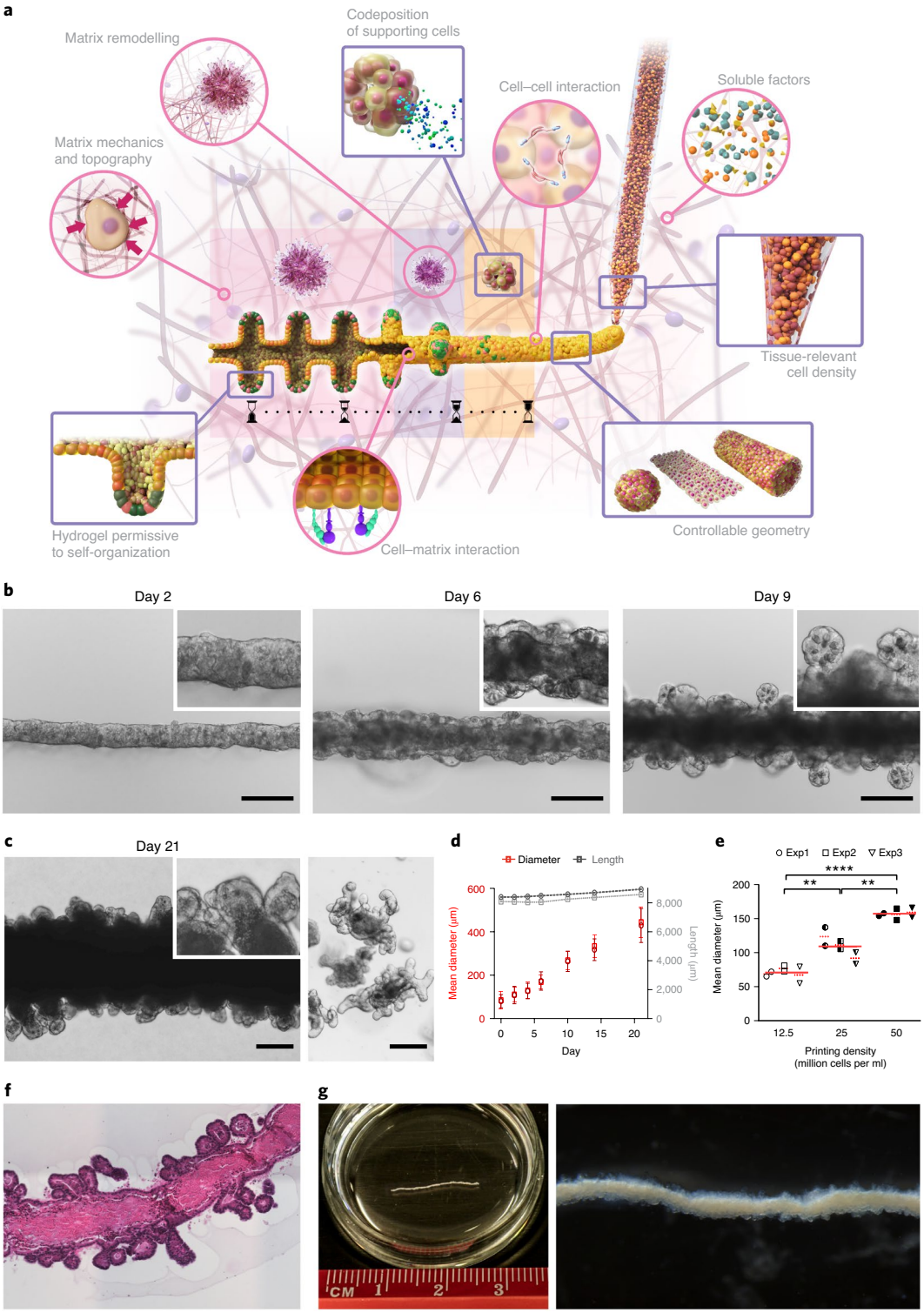

Fig. 2 | Macroscopic intestinal tube printing. a, Illustration of BATE applied to intestinal tissue engineering. Robust control over cellular density and tissue geometry can be achieved directly inside environments permissive to multicellular self-organization. **b**, Bright-field images of tube evolution. Insets show the dense condensation phase (day 2), the formation of a lumen and appearance of budding structures (day 6) and the formation of crypts with dark Paneth cells (day 9). Images are representative of $n > 10$ biologically independent experiments. Scale bars, 200 μm. **c**, Intestinal tube after 21 days of culture showing an intact epithelium despite large accumulation of dead cells (right) and classical organoid culture before passaging (right) for size comparison. Scale bars, 200 μm. **d**, For two tubes, mean tube diameter and total length versus number of days in culture. Standard deviation of the mean along the tube's length is indicated for the diameter. **e**, Influence of bioink cell density on tube diameter after 6 days of culture. Results of three different experiments are shown with two tubes for each. $^{**}P = 0.0074$ (left) and 0.0022 (right), $^{****}P < 0.0001$, determined by one-way ANOVA with Tukey's multiple comparisons test. **f**, Histological cross-section stained with Hematoxylin and Eosin to visualize the continuous lumen and cellular organization. Images are representative of $n = 3$ biologically independent experiments. Scale bar, 200 μm. **g**, Macroscopic images of intestinal tube spanning >15 mm. Images are representative of $n = 3$ biologically independent experiments.

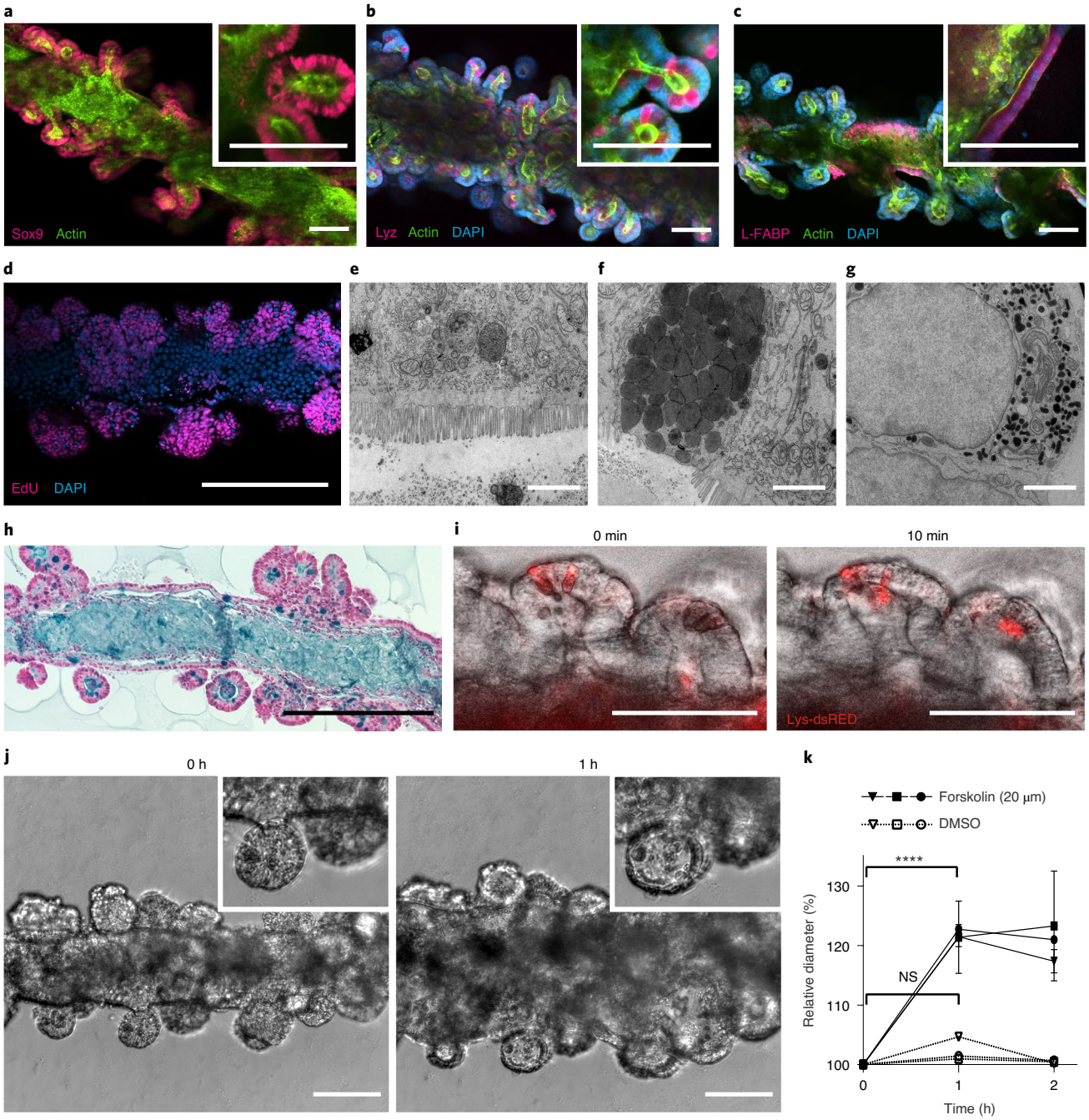

Fig. 3 | Intestinal tube characterization. a–c, Fluorescence confocal images of tubes, with a macroscopic and higher magnification view (insets) showing stem cells and progenitors (**a**), Paneth cells (**b**) and enterocytes (**c**). Cells are labelled with DAPI (blue), F-actin (green) and Sox9 (pink), Lyz (pink) or L-FABP (pink). Scale bars, 100 µm. **d**, Fluorescence confocal image (maximum intensity projection) showing proliferation using a 12-h EdU pulse (pink) and counterstained with DAPI (blue). Scale bar, 200 µm. **e–g**, Transmission electron microscopy of an intestinal tube section showing enterocytic brush border (**e**), goblet cells (**f**) and enteroendocrine cells (**g**). Scale bars, 2 µm. **h**, Alcian Blue and Nuclear Fast Red staining of the section of an intestinal tube showing mucus lining of the apical side of the epithelium and goblet cells. Scale bar, 200 µm. **i**, Lys-dsRED intestinal tube showing the position of the Paneth cells in the crypt structures of the tube (left) and the release of lysozyme granules in response to carbamylcholine treatment after 10 min (right). All micrographs in the figure are representative of $n = 3$ biologically independent experiments. Scale bars, 100 µm. **j**, Tube swelling in response to forskolin showing the morphology of a representative tube before (left) and 1 h after treatment (right). Scale bars, 100 µm. **k**, Graph showing the increase in diameter after forskolin treatment in function of the time. Results for three different experiments are shown, with two tubes each. Mean and standard deviation are shown. In each experiment a third tube exposed to dimethylsulfoxide was used as control. ****$P < 0.0001$, NS, $P = 0.7588$ determined by repeated measures two-way ANOVA with Tukey's multiple comparisons test.

ensure robust development and function, although existing cell culture and 3D printing approaches cannot reliably reproduce such physiological tissue–tissue interactions. BATE enables the sequential printing of multiple cell types to form complex geometries and cell-type arrangements with good spatial resolution (Fig. 4a–d). Given their important roles during intestinal develop-

ment and as a stem cell niche in vivo[21,22], we explored how mouse intestinal mesenchymal cells (IMCs) could be used to increase the relevance of bioprinted intestinal tubes (Fig. 2). We first tested the simultaneous printing of primary mISCs and IMCs in the same bioink deposited as a dense line (Fig. 4e–h). In this configuration, randomly dispersed IMCs were gradually excluded from the epithelial cell condensate to migrate at the periphery of the forming tube, self-sorting into an intestinal epithelium surrounded by supporting α-SMA-positive mesenchymal cells (Fig. 4e,f and Supplementary Video 6). The co-deposition of IMCs altered the initial phenotype of the self-organizing ISCs from a columnar and highly polarized epithelium to a more squamous one (Fig. 4e–h and Extended Data Fig. 9), mirroring previously described intestinal organoids cultured in the presence of intestinal myofibroblast feeder layers[23]. Incidentally, when the tubes were co-cultured with IMCs, complete lumen formation happened after only 1 day compared to 3–4 days without. The tube diameter also increased faster in the presence of IMCs, roughly doubling in size compared to control (Extended Data Fig. 9). Of note, after an initial radial expansion of the tube due to rapid fusion and proliferation, symmetry breaking still occurred, resulting in the highly stereotypical emergence of budding structures around the tube. That these budding structures represent de novo crypts was confirmed by the presence of Paneth cells, whereas differentiated cell types, such as enterocytes, were restricted to the non-budding areas (Fig. 4g,h). Similar results were obtained by printing IMCs in parallel lines around the mISCs, or by suspending the IMCs inside the gel before printing (Fig. 4i and Extended Data Fig. 9).

The versatility of BATE is also seen in its ability to control the sequential deposition of supportive cells spatially and temporally (Fig. 4i). Indeed, the integration of the bioprinter into an automated microscope makes it possible to track tissue emergence in real time and, if desired, return to specific locations to precisely place other cell types. Even though the fine nozzle is piercing the hydrogel during subsequent deposition, IMCs can still be deposited at any given time around the self-organizing epithelial tube to locally deliver key mesenchymal signals, for example. This presents the exciting possibility to guide tissue self-organization through cell-secreted temporal cues, potentially mirroring the action of native signalling centres as well as time-sensitive tissue–tissue interactions that may be critical during organ development.

One of the prevalent problems in stem cell-derived epithelial organoids is the physical inaccessibility of their lumen, restricting their lifetime and making it very difficult to study important physiological and pathological processes, such as host–microbe interactions or drug toxicity. In our system, the inclusion of stromal cells accelerates lumen formation and increases lumen diameter (Extended Data Fig. 9). This allows to connect the tissues to a liquid perfusion system to remove dead cells shed into the lumen during tissue turnover, a feature that could not be achieved with the densely filled lumen of intestinal organoids and intestinal tubes (Fig. 4j and Supplementary Video 7). This demonstrates how multicell-type bioprinting, in combination with extrinsically guided self-organization, can be leveraged to increase the relevance of tissue models.

Finally, we tested whether BATE could be used to establish multi-tissue models via combinatorial printing of various epithelial cell types from the gastrointestinal tract. Organoid-forming stem cells from different organs can be aspirated one after the other and dispensed sequentially to generate a cellular gradient flanked by two pure populations (Fig. 4a). Using this approach, stem cells from the stomach and colon, isolated from mTmG-mice that express membrane-localized dTomato protein, were combined with LGR5-eGFP mISCs to create large tubes featuring a gastrointestinal or small/large intestinal junction. Bright-field and fluorescence imaging revealed that the organ-specific identities were conserved after printing and throughout culture, ultimately resulting in a clear distinction between the intestinal zone filled with crypts containing LGR5^{+} stem cells, the smoother gastric or colonic zone, as well as the organ boundary where the crypt number progressively decreased (Fig. 4k,l and Extended Data Fig. 10). Gene expression analysis confirmed that both tissue identities are preserved within our multi-tissue models, with high expression of both small intestine (*Alpi*, *Lyz1*, *Muc2*) and gastric markers (*Muc5ac*, *Muc6*, *Pgc*) coexisting in the gastrointestinal tubes (Fig. 4m). BATE thus represent a powerful tool to answer unmet needs for multiple tissue or organ integration in organoid culture.

Efforts to create large-scale constructs out of organoids have been attempted by randomly positioning intestinal organoids inside a contracting collagen ring[24] or by punctually injecting mammary epithelial cells directly inside crosslinked collagen[25]. Here, we show how this concept of organoid fusion can be used to produce relatively large-scale tissues using identical building blocks, as well as mimic tissue boundaries by using building blocks from related organs. The local self-organization properties of organoid-forming stem cells can also be modulated by supportive cells to yield constructs with improved growth or altered development.

We believe that our cell-printing approach to guide tissue morphogenesis at different scales has several advantages compared to existing bioprinting technologies. Fragile cells such as primary stem cells can be organized into a complex geometry directly within the most potent 3D culture matrices, such as Matrigel. In comparison, previous studies have succeeded in printing cell-only bioink inside a support bath of microgels[6] or in printing biomaterial-based bioink directly inside self-healing guest–host hydrogels[7]. These strategies have, however, failed to provide the necessary environment for complex self-organization processes. In addition to enabling morphogenetic guidance using tissue–tissue interactions, BATE also reduces printing time and geometrical complexity because the microscopic architecture of the final constructs is created by the cells during subsequent remodelling and self-organization.

Fig. 4 | Co-culture printing. a–**d**, Micrographs of cells stained with cell tracker dyes showing the printing of cellular gradient (**a**), two different cell types within a dispersed third one (**b**), discontinuous lines (**c**) and complex multicellular pattern (**d**). Scale bars, 500 μm. **e**–**h**, Self-sorting of ISCs and IMCs during intestinal tube formation (**e**) IMCs stained with cell tracker (blue) are initially randomly dispersed within the ISCs (green, Lgr5–eGFP). **f**, SMA-positive IMCs (red) are located at the periphery of the tube. **g**,**h**, After 6 d, enterocytes are located on flatter surface and excluded from crypts (**g**) whereas Paneth cells are located within the crypts (**h**). Scale bars, 100 μm. **i**, Bright-field images of intestinal tube evolution with IMC patterning, demonstrating control over spatial (top) and temporal (bottom) deposition. Scale bars, 200 μm. **j**, Bright-field images of an intestinal tube before (top) and after (bottom) perfusion. Scale bars, 200 μm. **k**, Tubes composed of mouse stomach corpus (mT) and mouse small intestine (Lgr5–eGFP) stem cells directly after printing (left) and 6 d later (right). Scale bar, 500 μm. **l**, High-resolution image with insets representing the stomach part, the transition zone and the intestinal part. Scale bars, 500 μm. **m**, Heatmap of quantitative real-time PCR data showing the relative expression of stomach specific genes (*Muc5ac*, *Muc6*, *Pgc*), intestine specific genes (*Alpi*, *Lyz1*, *Muc2*) as well as *Chga* and stem/progenitor cells (*Lgr5*, *Sox9*) in tubes composed of one or both cell types 4 d after printing. Average expression over two tubes, normalized to organoids in standard culture conditions are shown (see Methods). As a comparison, gene expression levels for organoids originating from single cells and kept in the same medium as the tubes for the same time period are shown. All bright-field and fluorescent images in the figure are representative of $n = 3$ biologically independent experiments.

We believe that with BATE, local rules of cellular interactions and self-organization specific to a group of cells can be multiplied across different scales, provided that the geometry, cellular density, and the environment are suitable. As such, the conditions that have been optimized for different organoid systems can be seamlessly translated to the macroscopic scale by bioprinting the rel-

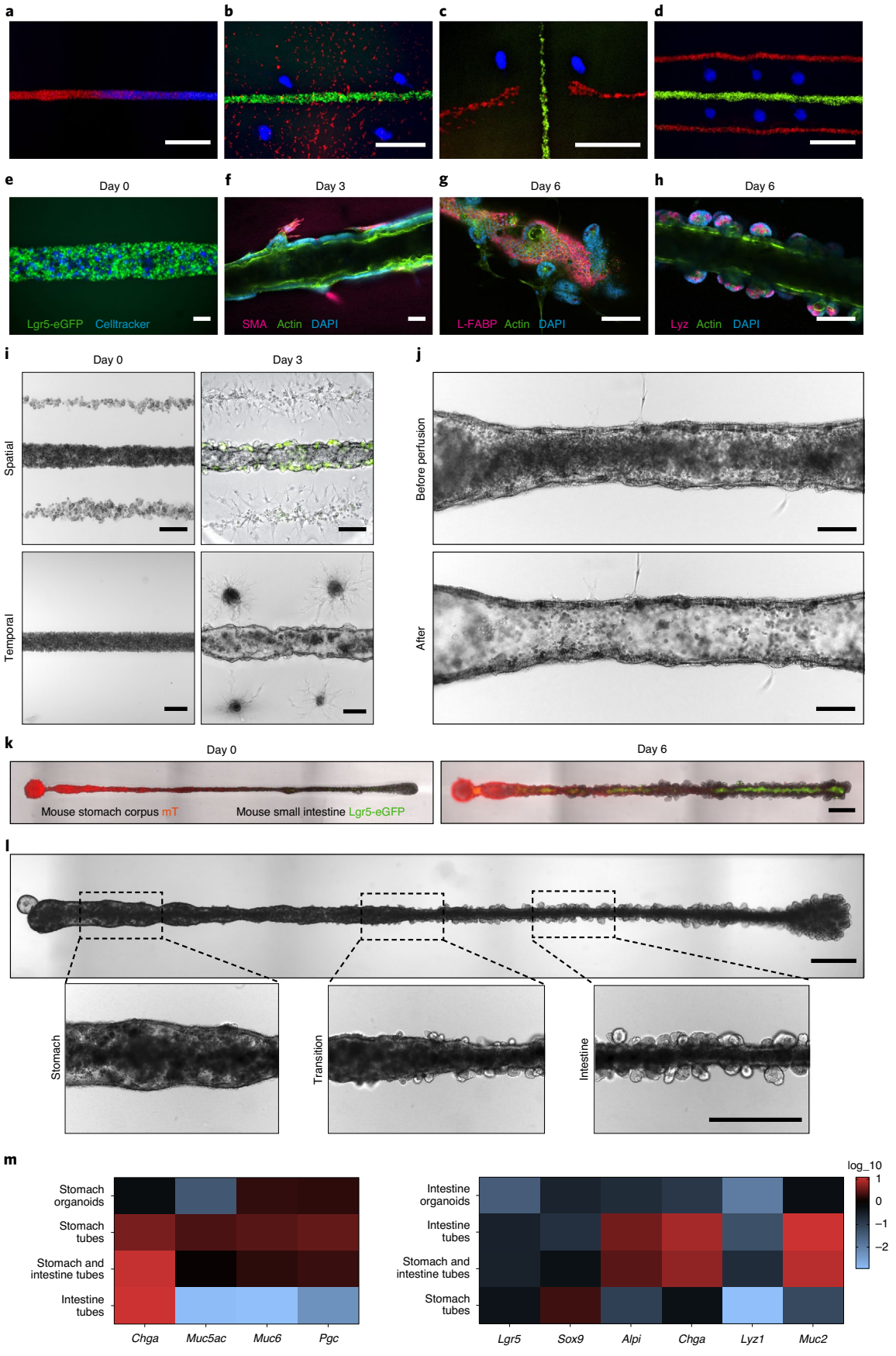

evant stem cells in their specific permissive environments. Because these fundamental concepts are broad, we envision that the same design strategy for naturally programmed building blocks could also be applied to tissues from different origins, combining existing organoid systems as well as their relevant supportive cells. This study thus opens new avenues in stem cell biology and regenerative medicine, providing a powerful tool for engineering self-organized tissues and mimicking organ boundaries as well as other tissue–tissue interactions. The fact that the cells contained within these printed tissues follow a well-regulated physiological morphogenetic program, contrary to the exaggerated spatial confinement or excessive restrictions seen in other bioprinting approaches, may also hold promise in substantially increasing their functionality, integration and maturation in vivo.

Online content

Any methods, additional references, Nature Research reporting summaries, source data, extended data, supplementary information, acknowledgements, peer review information; details of author contributions and competing interests; and statements of data and code availability are available at https://doi.org/10.1038/s41563-020-00803-5.

Received: 25 October 2019; Accepted: 17 August 2020;
Published online: 21 September 2020

References

1. Murphy, S. V. & Atala, A. 3D bioprinting of tissues and organs. *Nat. Biotechnol.* **32**, 773–785 (2014).
2. Liu, W. et al. Rapid continuous multimaterial extrusion bioprinting. *Adv. Mater.* **29**, 1604630 (2017).
3. Keriquel, V. et al. In situ printing of mesenchymal stromal cells, by laser-assisted bioprinting, for in vivo bone regeneration applications. *Sci. Rep.* **7**, 1778 (2017).
4. Hinton, T. J. et al. Three-dimensional printing of complex biological structures by freeform reversible embedding of suspended hydrogels. *Sci. Adv.* **1**, e1500758–e1500758 (2015).
5. Lee, A. et al. 3D bioprinting of collagen to rebuild components of the human heart. *Science* **365**, 482–487 (2019).
6. Bhattacharjee, T. et al. Writing in the granular gel medium. *Sci. Adv.* **1**, e1500655–e1500655 (2015).
7. Highley, C. B., Rodell, C. B. & Burdick, J. A. Direct 3D printing of shear-thinning hydrogels into self-healing hydrogels. *Adv. Mater.* **27**, 5075–5079 (2015).
8. Jamal, M. et al. Bio-origami hydrogel scaffolds composed of photocrosslinked PEG bilayers. *Adv. Healthc. Mater.* **2**, 1142–1150 (2013).
9. Villar, G., Graham, A. D. & Bayley, H. A tissue-like printed material. *Science* **340**, 48–52 (2013).
10. Clevers, H. Modeling development and disease with organoids. *Cell* **165**, 1586–1597 (2016).
11. Lancaster, M. A. & Knoblich, J. A. Organogenesis in a dish: modeling development and disease using organoid technologies. *Science* **345**, 1247125–1247125 (2014).
12. Laurent, J. et al. Convergence of microengineering and cellular self-organization towards functional tissue manufacturing. *Nat. Biomed. Eng.* **1**, 939 (2017).
13. Brassard, J. A. & Lutolf, M. P. Engineering stem cell self-organization to build better organoids. *Cell Stem Cell* **24**, 860–876 (2019).
14. Sato, T. et al. Long-term expansion of epithelial organoids from human colon, adenoma, adenocarcinoma, and Barrett's epithelium. *Gastroenterology* **141**, 1762–1772 (2011).
15. Blatchley, M. R. & Gerecht, S. Reconstructing the vascular developmental milieu in vitro. *Trends Cell Biol.* **30**, 15–31 (2020).
16. Sato, T. et al. Single Lgr5 stem cells build crypt-villus structures in vitro without a mesenchymal niche. *Nature* **459**, 262 (2009).
17. Sato, T. et al. Paneth cells constitute the niche for Lgr5 stem cells in intestinal crypts. *Nature* **469**, 415–418 (2011).
18. Es, J. Hvan et al. Enteroendocrine and tuft cells support Lgr5 stem cells on Paneth cell depletion. *Proc. Natl Acad. Sci. USA* **116**, 26599–26605 (2019).
19. Yokoi, Y. et al. Paneth cell granule dynamics on secretory responses to bacterial stimuli in enteroids. *Sci. Rep.* **9**, 2710 (2019).
20. Dekkers, J. F. et al. A functional CFTR assay using primary cystic fibrosis intestinal organoids. *Nat. Med.* **19**, 939–945 (2013).
21. Wells, J. M. & Spence, J. R. How to make an intestine. *Development* **141**, 752–760 (2014).
22. Stzepourginski, I. et al. CD34$^+$ mesenchymal cells are a major component of the intestinal stem cells niche at homeostasis and after injury. *Proc. Natl Acad. Sci. USA* **114**, E506–E513 (2017).
23. Farin, H. F., Van Es, J. H. & Clevers, H. Redundant sources of Wnt regulate intestinal stem cells and promote formation of Paneth cells. *Gastroenterology* **143**, 1518–1529.e7 (2012).
24. Sachs, N., Tsukamoto, Y., Kujala, P., Peters, P. J. & Clevers, H. Intestinal epithelial organoids fuse to form self-organizing tubes in floating collagen gels. *Development* **144**, 1107–1112 (2017).
25. Reid, J. A., Mollica, P. A., Bruno, R. D. & Sachs, P. C. Consistent and reproducible cultures of large-scale 3D mammary epithelial structures using an accessible bioprinting platform. *Breast Cancer Res.* **20**, 122 (2018).

Methods

Mouse strains. The following mouse lines were used for organ extraction and organoid culture establishment: 6–13-week-old heterozygous Lgr5–eGFP-IRES-CreERT2 (Jackson Laboratory), Lyz-dsRED[18], mTmG[26] or wild-type C57BL/6. All mouse work was conducted in accordance with animal experimentation protocols prescribed by EPFL and the Federation of European Laboratory Animal Science Associations. The establishment of organoid culture from mouse stomach, small intestines and colons was approved by the responsible ethical committee in compliance with local animal welfare laws, guidelines and policies.

Murine intestinal and colonic crypt isolation and culture. Murine intestinal crypts were isolated and cultured as previously described[14]. Briefly, the middle part of the intestine (roughly corresponding to the jejunum) was collected and washed thoroughly with ice-cold PBS without calcium and magnesium (Gibco) containing Gentamicin/Amphotericin (Gibco). Luminal content and villi were scraped with a glass slide to only keep the crypts and remove the rest of the epithelium. After washing with ice-cold PBS, intestinal sections were minced using two razor blades, collected in a 50-ml Falcon tube and washed again 5–10 times. The minced intestinal fragments were then incubated on ice for 20 min in PBS containing 20 mM EDTA (Gibco). After sedimentation of the fragments, EDTA was removed and replaced by PBS supplemented with 10% fetal bovine serum (FBS) (Gibco). The first fraction of the crypts was released by gentle vortexing of the tube and collected in another tube mounted with a 70-µm strainer (BD Bioscience). To collect the second fraction of the crypts, 10 ml of cold PBS was added, and intestinal fragments were triturated 10–20 times before being passed through a 70-µm strainer. The two fractions were analysed under the microscope and then combined and centrifuged at 100*g* before being resuspended in cold Advanced DMEM/F12 medium (Invitrogen). After a second centrifugation, crypts were resuspended in Matrigel (Corning, growth factor reduced, phenol red-free formulation), deposit as 20–25 µl droplets in 24-well plates and incubated for 10 min in hanging-drop position at 37 °C in 5% CO_2. After polymerization, 500 µl of organoid basal medium (Advanced DMEM/F12 containing GlutaMax, HEPES, penicillin-streptomycin, B27, N_2 (all from Invitrogen) and 1 µM *N*-acetylcysteine (Sigma-Aldrich)) was added and supplemented with 5 µm of Thiazovivin (Stemgent, only for the first 2 d), mEGF (50 ng ml^{-1}, Peprotech), Noggin (100 ng ml^{-1}, produced in-house), R-spondin (500 ng ml^{-1}, produced in-house), CHIR99021 (3 µM, Millipore) and valproic acid (1 mM, Sigma). Passaging of the cells was done every 3–4 d by mechanical disruption of the organoids through a glass pipet followed by reembedding in Matrigel. ISCs were maintained at 37 °C in 5% CO_2 humidified air during culture. Murine colonic crypts were isolated using the same protocol with longer EDTA incubation (30–40 min) and cultured in organoid basal medium supplemented with growth factors and small molecules, including mEGF, Noggin, R-spondin and CHIR99021 (same concentration as ISC culture) as well as Wnt3A (50 ng ml^{-1}, Time Bioscience) or in WNR-conditioned medium supplemented with mEGF (50 ng ml^{-1}) and Primocin (100 µg ml^{-1}, InvivoGen). Colon organoids were passaged every 5–7 d. Medium was changed every 2 d for all cultures.

Murine stomach gland isolation and culture. The extracted stomach was cut along the inner curvature, folded up and washed in PBS. The forestomach was removed, and the remaining glandular stomach split to the antrum and corpus part, respectively. Separately for both regions, the glands were extracted and cultured as organoids according a previously published protocol[27]. In brief, the stomach tissue was washed and minced in chelation buffer (sterile distilled water with 5.6 mM Na_2HPO_4, 8.0 mM KH_2PO_4, 96.2 mM NaCl, 1.6 mM KCl, 43.4 mM sucrose, 54.9 mM D-sorbitol, 0.5 mM DL-dithiothreitol, pH 7) and digested in EDTA-containing chelation buffer for 30 min at 4 °C with occasional swirling. Glands were extracted by applying mechanical pressure and subsequently separated from the larger fragments by letting the latter sediment in Advanced DMEM/F-12 medium. Glands and fragments thereof were seeded in Matrigel analogous to extracted intestinal crypts and cultured in WRN-conditioned medium supplemented with 1× B27, 1 mM *N*-acetylcysteine, 50 ng ml^{-1} of mEGF, 100 ng ml^{-1} of FGF 10 (Peprotech), 10 nM Gastrin (Tocris) and 0.5 mM Anaplastic lymphoma kinase (ALK)-inhibitor (A83-01, Tocris). Medium was replaced every 2–3 d. Passaging of the cells was done every 5–6 d by dissociation with TrypLE (Gibco) (4 min at 37 °C) followed by reembedding in Matrigel. During the initial phases of culture after initial seeding or after passaging, 10 µM Rho-associated, coiled-coil containing protein kinase (ROCK)-inhibitor (Y27632, Selleckchem) was added to the medium. During the first three passages, the medium was supplemented with Primocin.

Conditioned medium. Triple Wnt/R-Spondin/Noggin (WRN)-conditioned medium was produced using L-WRN cells (ATCC, CRL-3276) according to a modified version of a previously published protocol[28]. In brief, L-WRN cells were grown until confluency in Advanced DMEM/F-12 medium supplemented with 10 mM HEPES, 1× GlutaMax, 20% FBS and 50 U ml^{-1} of penicillin-streptomycin. After reaching confluency, medium was replaced and collected every 24 h for 9 d. Collections of three consecutive days were pooled and diluted 1:1 in fresh medium without FBS (final FBS concentration: 10%), sterile filtered and stored at −20 °C. Frozen aliquots were used within 4 months and kept at 4 °C for a maximum of 1 week after thawing. Cell lines HEK293 used to produce Noggin, R-spondin and Wnt conditioned medium were acquired from the Hubrecht Institute (Utrecht, Netherlands).

Murine myofibroblast isolation and culture. IMCs were isolated from 6–13-week-old C57BL/6 mice following a previously published protocol, with few modifications[29]. Briefly, the small intestine was prepared and used for intestinal crypt isolation as described in the corresponding section. Intestinal fragments were then washed and incubated in DMEM containing Collagenase IV (300 U ml^{-1}, Invitrogen) and Dispase (0.08 U ml^{-1}, Roche) for 30 min at 37 °C in a shaking water bath. The supernatant was then collected, centrifuged at 280*g* for 5 min and resuspended in DMEM supplemented with 10% FBS, penicillin-streptomycin, L-glutamine, non-essential amino acids and insulin-transferrin-selenium (Invitrogen). Cells were then transferred to culture flasks and medium was changed after cell adhesion (4–5 h) and every 2 d after. Cells were split 1:2 as needed and used between passages 3 and 8.

Human small intestinal organoid culture. Human small intestinal organoids were provided by the laboratory of H. Clevers (Hubrecht Institute) within the framework of a collaboration agreement. Human small intestinal organoids were cultured in human ISC expansion medium composed of 50% L-WRN-conditioned medium, supplemented with 1× B27 supplement (Gibco), 1 µM N-acetylcysteine (Sigma-Aldrich), 50 ng ml^{-1} EGF (Peprotech), 500 nM A83-01 (Tocris), 10 nM gastrin (Sigma-Aldrich), 10 mM nicotinamide (Sigma-Aldrich), 10 µM SB202190 (Seleckchem), 10 nM prostaglandin E2 (Tocris). Y-27632 (10 µM, Seleckchem) was used in the first 48 hours after single-cell dissociation to prevent detachment-induced cell apoptosis. The medium was changed every two days and the expanding organoids were passaged every six to eight days by mechanical dissociation using a fire-polished glass Pasteur pipette. Organoids were used between passage number 10 and 20.

Cell lines. C2C12 cells (ATCC) were maintained in DMEM supplemented with 10% FBS, L-glutamine, sodium pyruvate, HEPES and penicillin-streptomycin (all from Invitrogen). HUVECs (Lonza) were maintained using EGM-2 Bulletkit medium (Lonza) and used until passage 10. To trigger angiogenesis, VEGF (50 ng ml^{-1}, R&D systems) was added. hMSCs (Lonza) were obtained as passage 1 cells and expanded up to passage 10 in αMEM supplemented with 10% FBS, 2 mM GlutaMax, 100 U ml^{-1} of penicillin and 100 µg ml^{-1} of streptomycin (all from Gibco) and human FGF2 (1 ng ml^{-1}, Peprotech). Medium was changed every 2 d for all cultures.

Bioprinting hardware. All 3D printing was performed on a custom-built extrusion-mode printer fabricated by combining a syringe pump (neMESYS, Cetoni) with either a Zeiss Axiovert 200 M microscope or a Nikon Eclipse Ti inverted microscope. During the printing processes, the microscope controller was used to precisely control the positions, while the syringe pump was used to control the flow of the extruded cell suspension. For the nozzle, a PCR micropipette (Drummond) was pulled using a DMZ micropipette puller (Zeitz Instruments) using empirically defined settings for optimal printing. The pulled glass capillaries have a long conical taper that can be broken by carefully applying pressure on the tip at the desired position, obtaining the internal diameter needed for the printing of beads, cells or aggregates. The long taper ensures lower deformation of the surrounding environment when printing. Nozzle with internal diameters ranging from 20 to 200 µm were fabricated depending on the needs, examined under a microscope to ensure a clear and homogeneous cut, treated with Sigmacote (Sigma-Aldrich) to prevent adhesion of the cells for a few minutes and dried for several hours. The glass capillary was then bended under a flame and connected to 1/16" polyetheretherketone tubing with a dual small hub RN coupler and RN compression fittings for glass capillary and polyetheretherketone tubing (all from Hamilton). The connector was arranged in between a polydimethylsiloxane (PDMS) slab and a glass slide to increase stability and an easy mounting part was fabricated using reverse moulding of the condenser in PDMS. The perfectly fitting PDMS block then allowed mounting of the nozzle in the field of view of the microscope by bonding of the PDMS with the glass slide holding the nozzle. The microscope heating/cooling system 'the cube' (Life Imaging Services) was used to maintain the environment at the desired temperature.

Bioprinting process. *Hydrogel precursor preparation.* For the hydrogel precursor mixture, a native bovine dermis collagen type I solution (5 mg ml^{-1}, Kouken) was neutralized and reconstituted on ice with 10% v/v of 10× DMEM (Invitrogen), 8% Advanced DMEM/F12 medium, 2% v/v of sodium bicarbonate 0.5 M to a 4 mg ml^{-1} final solution. The collagen solution was mixed with ice-cold Matrigel in the following ratios: 50% for beads, 50% for MSCs, 0–50% for experiments on matrix stiffness, 20% for intestinal, stomach and colon stem cells, 100% collagen for HUVECs.

Cell preparation. Single-cell suspensions were prepared following established protocol for the different cell types. Briefly, IMCs, HUVECs, MSCs and C2C12

were washed with PBS and incubated with TripLE Express (Life Technologies) for 3–5 min at 37 °C. Cells were then collected in a 15-ml Falcon tubes with culture medium containing 10% FBS and filtered through a 40-µm strainer to avoid clogging of the nozzle by cell aggregates. Cells were centrifuged and resuspended in their respective medium supplemented with 1.5 mM EDTA.

Stomach, intestinal and colon organoids were dissociated at 37 °C for 8 min (mouse stomach and intestine) or 15–17 min (human intestine, mouse and human colon) using TrypLE Express supplemented with DNase I (2,000 U ml^{-1}; Roche), *N*-acetylcysteine (0.5 mM) and Y27632 (10 µM). Cells were also passed through a cell strainer and resuspended in ENR or WNR-conditioned medium supplemented with EDTA (2 mM). For mouse colon stem cells, an extra 10% FBS was added. Cells were kept on ice until printing.

Cells were resuspended at concentrations ranging from 10^7 to 10^8 cells per ml to be used for printing.

For organoid printing, organoids were retrieved from the Matrigel 2 d after having been seeded as single cells. Matrigel was mechanically disrupted using cold organoid basal medium, collected in a Falcon and centrifuged (200*g*, 4 min, 4 °C). The supernatant was removed, and organoids were washed once more with cold basal medium. They were then incubated with Dispase (0.08 U ml^{-1}) and Collagenase IV (10%), *N*-acetylcysteine (0.5 mM) and Y27632 (10 µM) at 37 °C for 5 min. The organoids where then washed three times with basal medium and resuspended in ENR supplemented with EDTA.

Bioprinting. Two small rectangular 2–3-mm-thick PDMS spacers were cut, sterilized with ethanol and placed on the bottom of 6- or 12-well plates to reduce the amount of hydrogel used for printing. The nozzle was washed for several minutes in ethanol and then rinse thoroughly with sterile water or PBS before printing. A droplet of cell suspension (5–10 µl) was place in an empty well before being aspirate by the nozzle at a volumetric flow rate of 50–100 µl s^{-1}. The ice-cold hydrogel was then added in between two PDMS blocks before starting to print. Cells were dispensed directly in the hydrogel by extrusion of the suspension at a volumetric flow rate of 15–100 µl s^{-1} depending on the cellular density and geometrical thickness desired. For hydrogels that are too liquid at low temperature (4 °C), the temperature can be controlled in the bioprinting periphery to obtain optimal viscosity. The user can print for 2–5 min before the nozzle starts dragging the gelling hydrogel too much. Cellular density, flow rate and stage speed can then be modulated depending on the construct to print. For example, the standard intestinal and gastrointestinal tubes were generated using a 90–100-µm nozzle diameter, a cell density of 50 million cells per ml, a flow rate of 35 nl s^{-1} and a temperature of 25–32 °C. For multiple cell printing, sequential aspirations and depositions were used depending of the printing (gradient or separate prints). Tissue geometries were printed directly by the user controlling the stage while looking through the microscope. The embedded construct was incubated for 10 min at 37 °C to finalize crosslinking before adding the medium with the intended growth factors. For intestinal, stomach and colon stem cells the Rock inhibitor Thiazovivin (2.5 µM) was added to the medium for the first 2 d to prevent anoikis.

Epithelial tubes were cultured using the following medium: mouse intestine (organoid basal medium + mEGF, Noggin, R-spondin), stomach (WNR-conditioned medium + B27, *N*-acetylcysteine, Gastrin, mEGF, FGF10 and A83-01), colon (WNR-conditioned medium + mEGF and Primocin), coculture of stomach and intestine (WNR-conditioned medium + Gastrin, mEGF and FGF10) and coculture of intestine and colon (WNR-conditioned medium + mEGF and Primocin), human intestine expansion medium (EGF, 10% Noggin-conditioned medium, 25% R-Spondin-conditioned medium, 50% Wnt3a-conditioned medium, nicotinamide, gastrin, A83-01, SB202190, prostaglandin E2), human intestine differentiation medium (EGF, 10% Noggin-conditioned medium, 25% R-Spondin-conditioned medium, gastrin, A83-01), using the same concentration as described above. Medium was changed every two days for all cultures.

Matrix degradation. Collagenase type IV was diluted at 5 mg ml^{-1} (1,450 U ml^{-1}) directly into the relevant medium before being used as a 10× concentrated solution that could be directly added to the wells of the printed constructs. The printouts were treated with collagenase for 12 min, washed twice with PBS and put back in their growth medium.

Temporal deposition. Printed intestinal constructs were put back under the microscope coupled to the bioprinter with temperature controlled at 37 °C. A droplet of IMCs (0.5×10^8 cells per ml) was then deposited on an adjacent well and aspirated. The user can navigate the previous printouts and deposit cells inside the hydrogel by looking into the microscope and manually adjusting the height of the nozzle. Dots of IMCs were patterned by lifting the nozzle and punching through the hydrogel before deposition. A programmed syringe push allowed the deposition of a similar number of cells for every injection. Of note, the hydrogel was locally disrupted by the nozzle, but did not preclude cellular deposition if cellular density was high enough.

Cell viability measurements. C2C12 and HUVECs were printed according to the protocol described above. For qualitative imaging, the constructs were then incubated with calcein AM (4 mM) and Ethidium homodimer-1 (2 mM) for 30–40 min following the live/dead kit instructions (Thermo Fisher Scientific). Incubation was done on different printouts at different time points with 30 min incubation in saponin (0.3%) for positive staining of dead cells. Pictures were taken after washing twice with PBS. For quantitative imaging, constructs were stained with Hoechst 33342 (5 µg ml^{-1}, Thermo Fisher Scientific) and Ethidium homodimer-1 (2 mM, Thermo Fisher Scientific), because calcein AM did not allow to distinguish single cells after considerable remodelling and thus hindered precise cell counting. Three different printing experiments ($n = 3$) were performed for each cell line and time point (immediately after printing, and after 24 h).

Multiple cell printing using cell trackers. C2C12 cells were incubated with calcein AM, Cell tracker deep red dye or Cell tracker blue dye (all from Thermo Fisher Scientific) following the manufacturer's protocols. Cell tracker blue was used at a final concentration of 10 µM, whereas deep red cell tracker was diluted to a final concentration of 1 µM and calcein AM was used at 4 mM. Cells were washed and incubated with their respective cell trackers during 30 min at 37 °C, then dissociated and prepared for printing as detailed before. Pictures were taken after ECM gelation and medium addition.

Forskolin and carbamylcholine treatment. Tubes with crypt structures (days 6–8) were treated with forskolin (20 µM, Selleckchem), carbamylcholine (100 µM, Sigma) or dimethylsulfoxide (Thermo Fisher Scientific).

Immunofluorescence staining. Printed constructs were rinsed twice with PBS and fixed with 4% paraformaldehyde (Thermo Fisher Scientific) in PBS for 25 min at room temperature. Following fixation, tissues were transferred onto glass slides with a homemade PDMS spacer and permeabilized with 0.2% Triton X-100 in PBS for 1 h at room temperature. They were then blocked with 10% goat serum in PBS containing 0.01% Triton X-100 for 3 h at room temperature. The samples were then incubated for 36 h at 4 °C with the primary antibody diluted in blocking buffer against lysozyme (1:50; Thermo Fisher Scientific), L-FABP (1:50; Santa Cruz) or Sox9 (1:50; Abcam) for intestinal tubes, CD31 (1:200; Cell Signalling Tech) for vascular tubes and alpha smooth muscle actin (1:100; Agilent) for IMCs. After washing for 3–5 h at room temperature, samples were incubated overnight at 4 °C with secondary antibody Alexa 647 donkey-α-rabbit (1:500 in blocking solution; Invitrogen) or Alexa 647 donkey-α-mouse (1:500 in blocking solution; Invitrogen), DAPI (1:2,000) and phalloidin-Alexa 488 (1:200; Invitrogen). After at least 3 h of washing, samples were mounted in fluoromount-G (Thermo Fisher Scientific) before imaging. Proliferative cells were stained with a Click-iT EdU Alexa Fluor 647 imaging kit (Thermo Fisher Scientific) following the manufacturer's instructions.

Microscopy and image processing. Bright-field and fluorescent (mT, green fluorescent protein (GFP), dsRED, viability die, cell trackers) images of printouts were taken using a Nikon Eclipse Ti inverted microscope system equipped with a ×4/0.20 numerical aperture (NA), ×10/0.30 NA and ×20/0.45 NA air objectives; 395-, 470-, 555- and 632-nm filters and controlled by NIS software or a Leica SP8 system equipped with a ×10/0.30 NA air objective, a ×25/0.95 NA water objective, a 440-nm pulsed laser (40 MHz–312.5 kHz) as well as a Supercontinuum White Light Laser (80–10 MHz + Manual) controlled by LEICA LAS-X software. Fixed samples were imaged with an inverted confocal microscope (INVERT Zeiss Axio Observer Z1) equipped with ×10/0.30 NA and ×20/0.80 NA air objectives; 405-, 488- and 555-nm lasers and controlled by ZEN 2009 imaging software (Zeiss). Image processing was performed using Fiji/ImageJ (NIH) and further processed using Photoshop CC (Adobe) using only standard contrast and intensity level adjustments. Animated videos were rendered using Premiere Pro (Adobe).

Tube diameter analysis. A tiled image of the tube was taken with stored position for imaging on multiple days. Image analysis was carried out using the following pipeline in Fiji. Images of the same tubes at different time points were stacked and registered using the StackReg plugin (Rigid Body). Then a segmented line with a width larger than the tube was draw along the tube and used to straighten it. This line was saved and used for each image of the stack, which were further processed independently. Each image was filtered using Subtract Background. An automatic threshold was applied to the image and it was converted to mask and holes were filled if required. The plugin Local Thickness was run on this mask. Eventually, an horizonal line separating the image exactly in the middle was drawn and the profile of the tube along that line was measured and saved.

Statistics. Graphs and statistical analysis were made in GraphPad Prism. For the influence of cell density on tube diameter, a one-way analysis of variance (ANOVA) with Tukey's multiple comparisons test was performed, comparing the mean diameter of tubes at day 6 after printing. The experiment was repeated three times, each with two tubes per density and values were averaged per experiment before being compared. Test details were as follows: 50×10^6 cells per ml versus 25×10^6 cells per ml, $q = 8.555$ d.f. $= 6$; 50×10^6 cells per ml versus 12.5×10^6 cells per ml, $q = 15.3$ d.f. $= 6$ and 25×10^6 cells per ml versus 12.5×10^6 cells per ml, $q = 6.745$ d.f. $= 6$. For forskolin-induced swelling, a repeated measures two-way ANOVA with Tukey's multiple comparisons test was performed, comparing the increase in tube diameter for the control and for the treated condition between

before and 1 h after the treatment. Tubes were used 8 d after printing and from three different experiments, each with one control and two treated tubes. For the treated condition, values were averaged per experiment before being compared. Test details are as follows. For the control sample: before treatment versus 1 h after treatment, $q = 2.887$ d.f. = 2; before treatment versus 2 h after treatment, $q = 4.862$ d.f. = 2 and 1 h after treatment versus 2 h after treatment, $q = 2.111$, d.f. = 2. For the treated sample: before treatment versus 1 h after treatment, $q = 72.77$ d.f. = 2; before treatment versus 2 h after treatment $q = 16.86$ d.f. = 2 and 1 h after treatment versus 2 h after treatment $q = 1.075$ d.f. = 2. For the evolution of the tube diameter over 3 weeks, the mean and the standard deviation of the diameter as well as the length were plotted for each tube.

Histology. Samples were prepared together with the EPFL Histology Core Facility in accordance with their standard procedures. Briefly, samples were fixed in 4% paraformaldehyde overnight at 4 °C and washed three times with PBS. Fixed samples were placed on an even surface and covered by HistoGel (Thermo Fisher Scientific) previously heated to 50 °C. The sample was then cooled before being embedded in paraffin as standard protocol. Sectioning was done on a Leica cryostat CM3050S at −30 °C. For staining, the 10-µm sections were either immersed in Alcian Blue pH 2.5 solution for 25 min and counterstained with Nuclear Fast Red, or immersed in Hematoxylin Eosin solution. Samples were then dehydrated and mounted with xylene-based glue. Sections were imaged on a LEICA DM 5500 microscope, DMC 2900 Color camera. Image processing was made in ImageJ (NIH).

Transmission electron microscopy. Samples were chemically fixed in a buffered mix of 2.5% glutaraldehyde and 2.0% paraformaldehyde in 0.1 M phosphate buffer (pH 7.4), and left for 4 h. Then samples were washed thoroughly with cacodylate buffer (0.1 M, pH 7.4), postfixed for 40 min in 1.0% osmium tetroxide with 1.5% potassium ferrocyanide, followed by 40 min in 1.0% osmium tetroxide alone. They were finally stained for 30 min in 1% uranyl acetate in water before being dehydrated through increasing concentrations of alcohol and then embedded in Durcupan ACM (Fluka) resin. The samples were then placed in moulds and the resin polymerized at 65 °C for 24 h. Thin sections of 50-nm thicknesses were cut with a diamond knife, and collected onto single slot copper grids with a pioloform support film. Sections were contrasted with lead citrate and uranyl acetate, and images taken with a transmission electron microscope at 80 kV (Tecnai Spirit, FEI Company with Eagle CCD camera).

Perfusion set-up. Sterile scissors were used to create two clear cuts at the extremities of the intestinal tubes. The intestinal tubes were then placed under the microscope with the bioprinter and kept at 37 °C and 5% CO_2 during the perfusion process. The perfusion nozzle was prepared such as the printing nozzle but was made smaller (~50 µm) and bent in a Z shape. This nozzle was mounted on the bioprinter and inserted inside the intestinal tubes using the manually controlled stage. Perfusion was controlled by a house-made LabVIEW (National Instruments) interface linked to neMESYS software (Cetoni).

For endothelial tubes, a glass nozzle (tip, 30 µm) was mounted on a mouth pipetting device and the perfusion process controlled by hand. Then 2,000-kDa of luorescein isothiocyanate dextran (Invitrogen) or 0.1 µm of red fluorescent beads (Invitrogen) diluted in cell culture medium were injected.

Real-time quantitative PCR (qPCR). Stomach and intestinal organoids in Matrigel were collected using the RLT buffer from the RNeasy Micro Kit (Qiagen) supplemented with 40 mM dithiothreitol (Sigma). Tubes printed in Matrigel collagen mix were collected according to the following protocol: one wash with cold organoid medium, 3 min incubation at 37 °C with 200 µl Collagenase IV (300 U ml^{-1}), one wash with PBS 1× and RLT buffer supplemented with dithiothreitol. The lysates were then kept at −80 °C until further processing. The RNA extraction was performed using a RNeasy Micro Kit and complementary DNA were synthesized using the iScript cDNA Synthesis Kit (Bio-Rad) on a UnoCycler (WVR). Real-time qPCR was carried out using the Power SYBR Green PCR Master Mix (Applied Biosystems) on a QuantStudio 6 machine (Applied Biosystems). Primers are listed in Supplementary Table 1.

Reporting Summary. Further information on research design is available in the Nature Research Reporting Summary linked to this article.

Data availability

The datasets supporting the conclusions of this article are included within the article and its additional files. Source data are provided with this paper.

References

26. Muzumdar, M. D., Tasic, B., Miyamichi, K., Li, L. & Luo, L. A global double-fluorescent Cre reporter mouse. *Genesis* **45**, 593–605 (2007).
27. Bartfeld, S. & Clevers, H. Organoids as model for infectious diseases: culture of human and murine stomach organoids and microinjection of *Helicobacter pylori*. *J. Vis. Exp.* https://doi.org/10.3791/53359 (2015).
28. Miyoshi, H. & Stappenbeck, T. S. In vitro expansion and genetic modification of gastrointestinal stem cells as organoids. *Nat Protoc.* **8**, 2471–2482 (2013).
29. Koliaraki, V. & Kollias, G. Isolation of intestinal mesenchymal cells from adult mice. *Bio-Protocol* **6**, e1940 (2016).

Acknowledgements

We thank N. Gjorevski and A. Martinez Arias for valuable feedback on the manuscript. We thank S. Li and D. Dutta for deriving organoid lines from intestinal tissues of mTmG and Lys-dsRED reporter mice, respectively. We thank O. Mitrofanova for help with human intestinal organoid culture and tube printing, S. Giger for providing hMSCs and A. Manfrin and A. Chrisnandy for the qPCR primers for intestinal genes. We thank R. Guiet and O. Burri from EPFL's BioImaging and Optics Platform for help with intestinal tube analysis. We thank J. van Es and H. Clevers for providing intestinal tissues of Lys-dsRED reporter mice and J. McKinney for providing intestinal tissues of mTmG reporter mice. This work was funded by support from the EU Horizon 2020 Project INTENS (no. 668294-2), the Swiss National Science Foundation research grant no. 310030_179447, the National Center of Competence in Research (NCCR) 'Bio-Inspired Materials' (https://www.bioinspired-materials.ch/), the PHRT-PM/PH Research Project Proposal 2017, the Wellcome Trust Collaborative Award 211944/Z/18/Z, and EPFL.

Author contributions

M.P.L. and M.N. conceived the initial idea. J.A.B., M.N., T.H. and M.P.L. conceived the study, designed experiments and analysed the data. M.P.L. and J.A.B. wrote the manuscript. T.H. performed multi-gastrointestinal cell-type printing. M.H. was involved in performing and analysing stomach tube printing experiments. All authors provided feedback on the manuscript.

Competing interests

The authors declare no competing interests.

Additional information

Extended data is available for this paper at https://doi.org/10.1038/s41563-020-00803-5.

Supplementary information is available for this paper at https://doi.org/10.1038/s41563-020-00803-5.

Correspondence and requests for materials should be addressed to M.P.L.

Reprints and permissions information is available at www.nature.com/reprints.

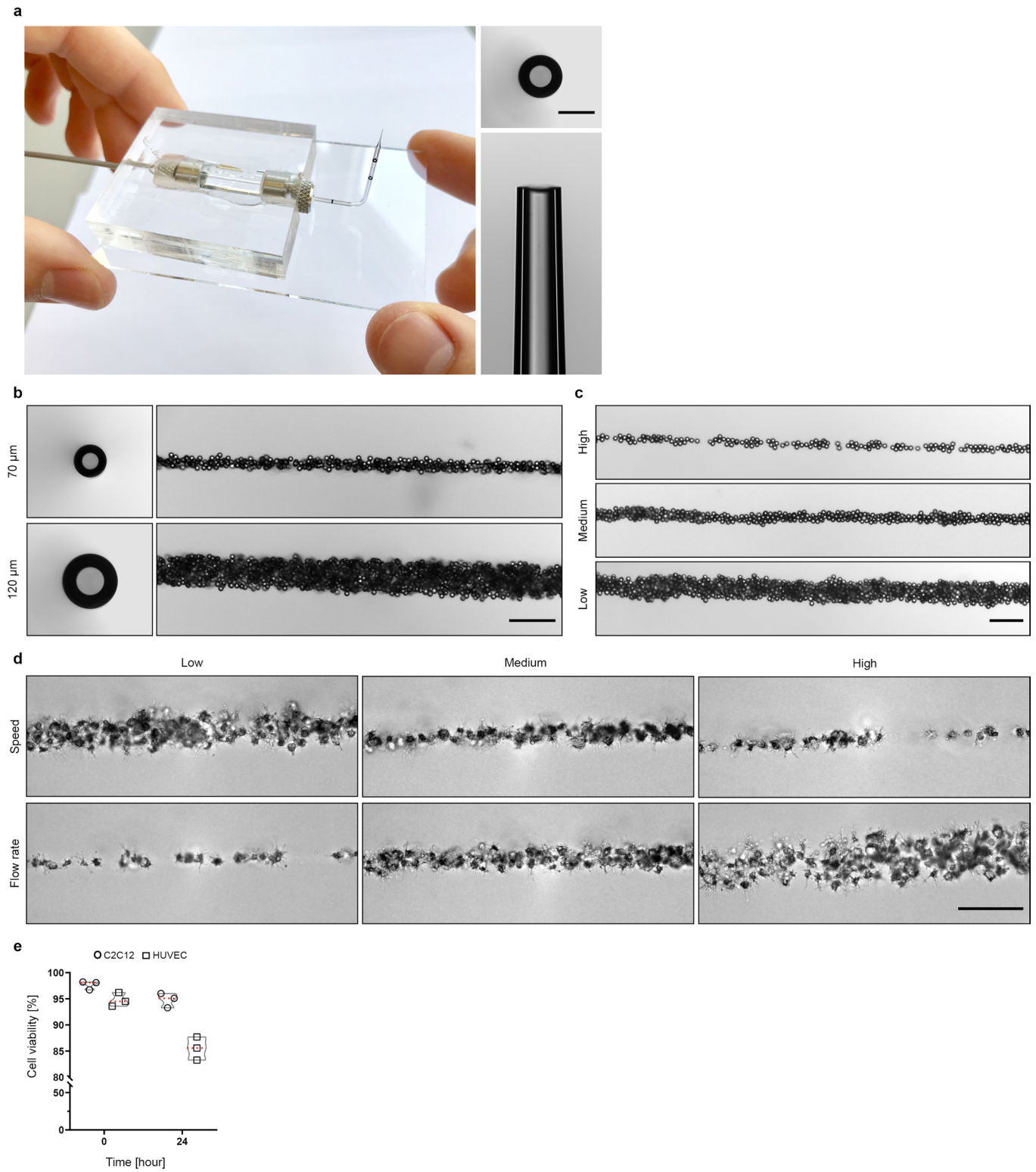

Extended Data Fig. 1 | Bioprinter set-up and proof-of-concept. Picture of the nozzle to be mounted on the microscope. The nozzle after pulling and breaking of the tip has a long taper and a clear cut. Scale bar, 200 µm. **b**, Printing with beads showing that resolution and printing thickness can be modulated by changing the nozzle size or (**c**) the speed of the stage movement. Images are representative of n = 3 independent experiments. Scale bars, 200 µm. **d**, Printing with HUVECs showing that resolution and cell density can be controlled by modifying the flow rate (syringe-based extrusion) or the printing speed (stage movement). Images are representative of n = 3 biologically independent experiments. Scale bar, 200 µm. **e**, Viability of C2C12 (circles) and HUVECs (squares) right after printing and 24 hours later. Data represented as percentage of live cells for three replicates (n = 3 biologically independent experiments), with the mean for each condition shown as a dotted line.

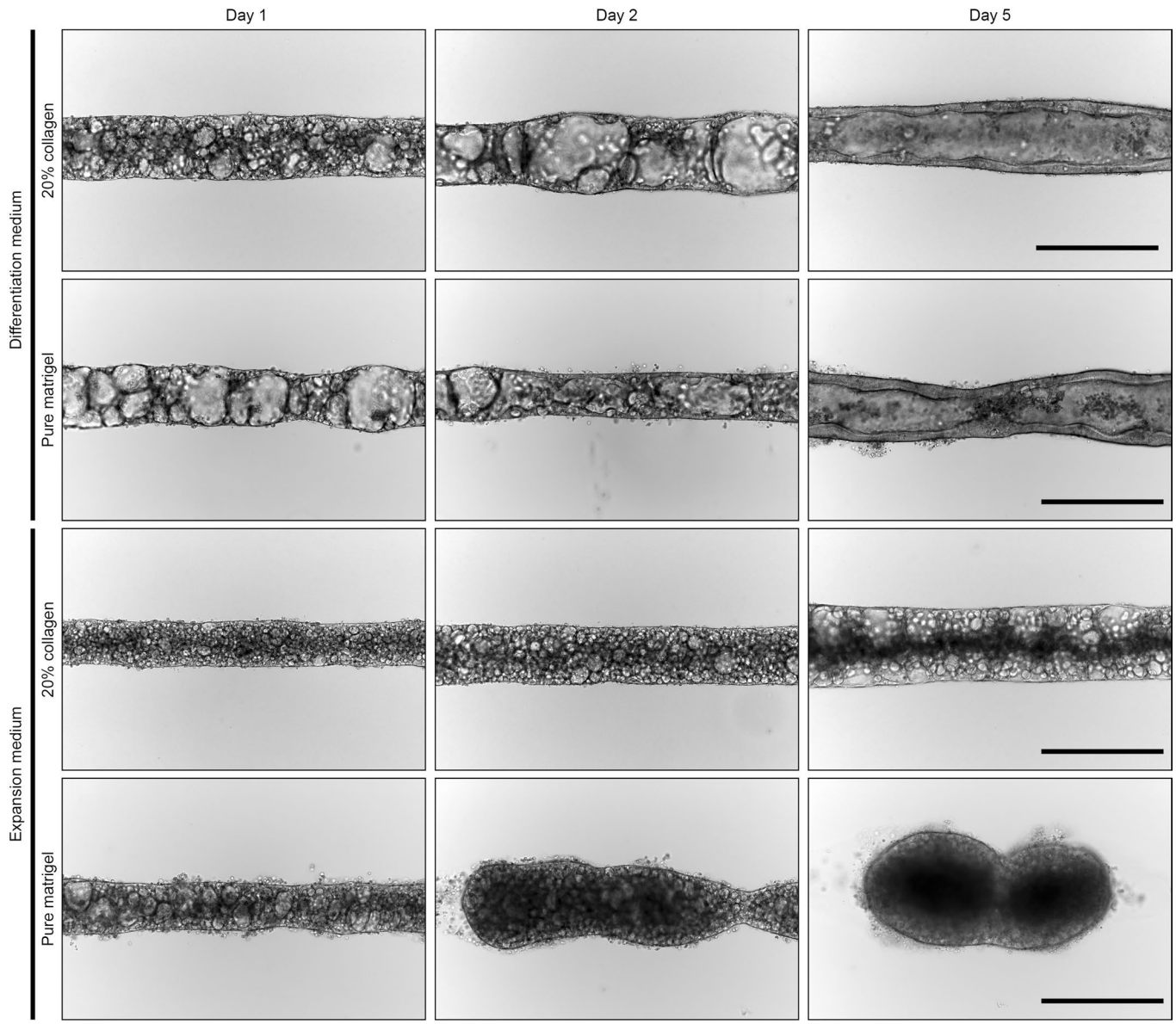

Extended Data Fig. 2 | Printing human intestinal tubes. Bright-field images showing the evolution of human intestinal stem cells printed as a line. Differentiation medium promotes the rapid formation of a continuous lumen. Increasing the matrix stiffness, by addition of collagen in the support hydrogel, allows to maintain the printed geometry better, preventing collapse of the tube due to cell-mediated matrix remodelling. Images are representative of n = 3 biologically independent experiments. Scale bars, 500 μm.

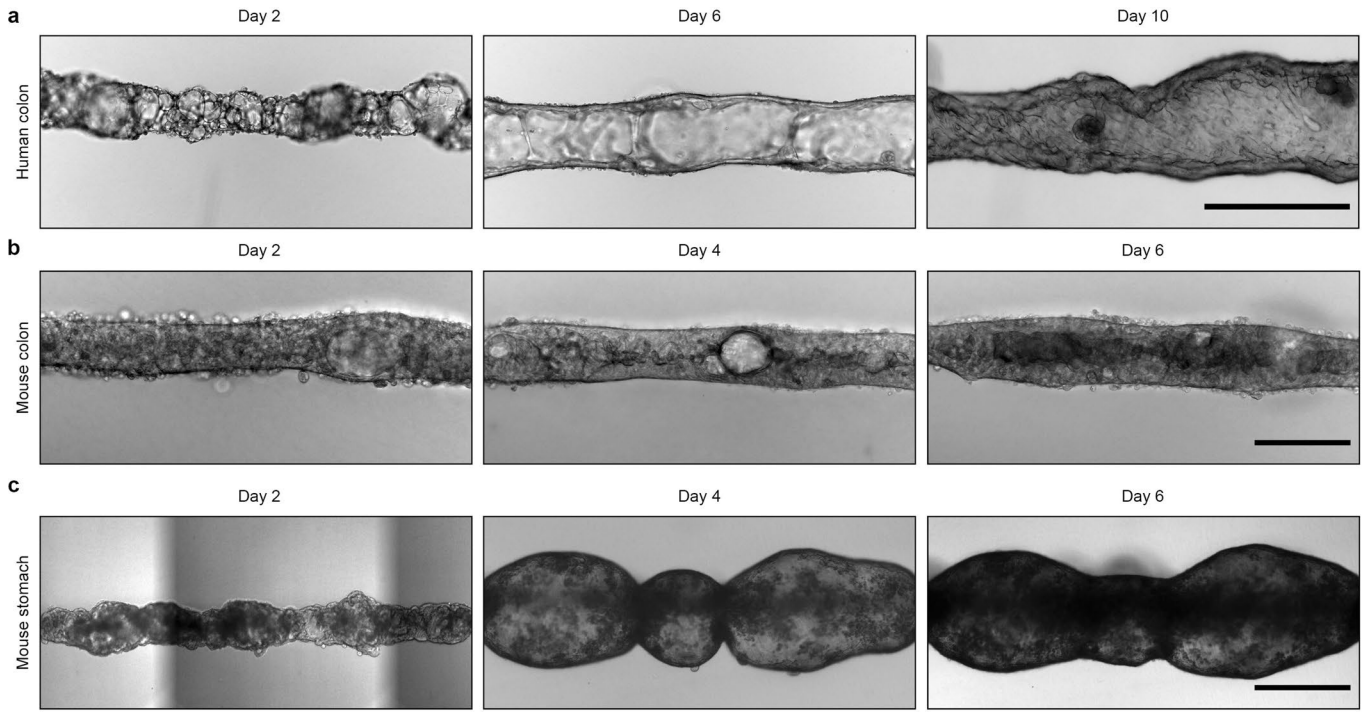

Extended Data Fig. 3 | BATE of colon and stomach epithelial tubes from mouse and human primary cells. a, Bright-field images of tube evolution from human and (**b**) mouse colon stem cells and (**c**) mouse stomach stem cells. In all cases, a thick tubular epithelium is formed by colony growth and fusion at high density. Images are representative of n = 3 biologically independent experiments. Scale bars, 500 μm.

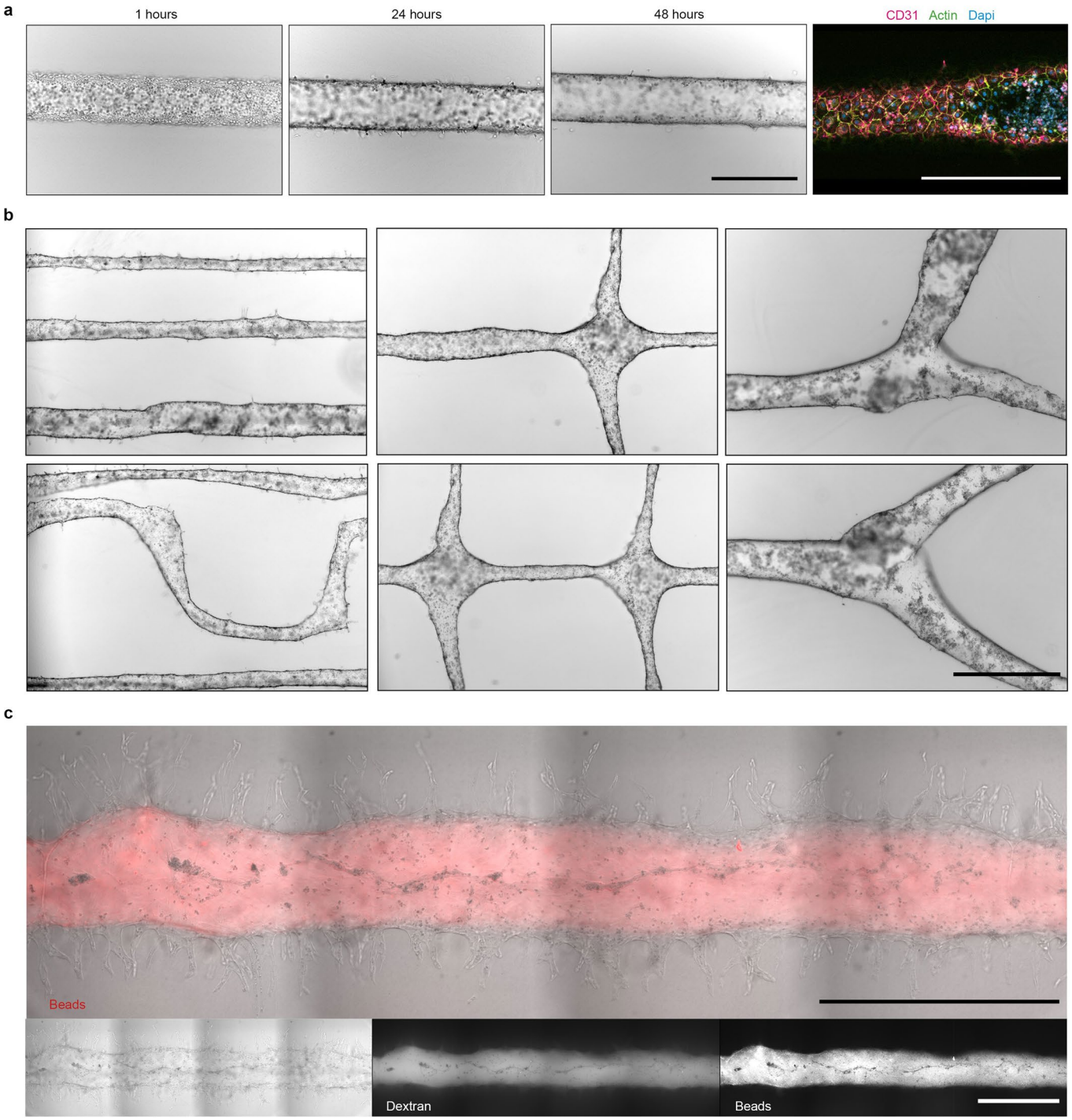

Extended Data Fig. 4 | BATE of vascular endothelial tubes. a, Evolution of a printed line of HUVECs, showing rapid reorganization into an endothelial tube with a single macroscopic lumen. Images are representative of n = 3 biologically independent experiments. Scale bars, 500 μm. **b**, Different geometries can be printed to form branched vascular tubes and other complex structures. Images are representative of n = 3 biologically independent experiments. Scale bar, 1000 μm. **c**, Bright-field and fluorescent images showing vascular tube perfusion with fluorescently labelled dextran (2000 kDa) or fluorescently labelled beads (0.1 μm). Images are representative of n = 3 biologically independent experiments. Scale bars, 1000 μm.

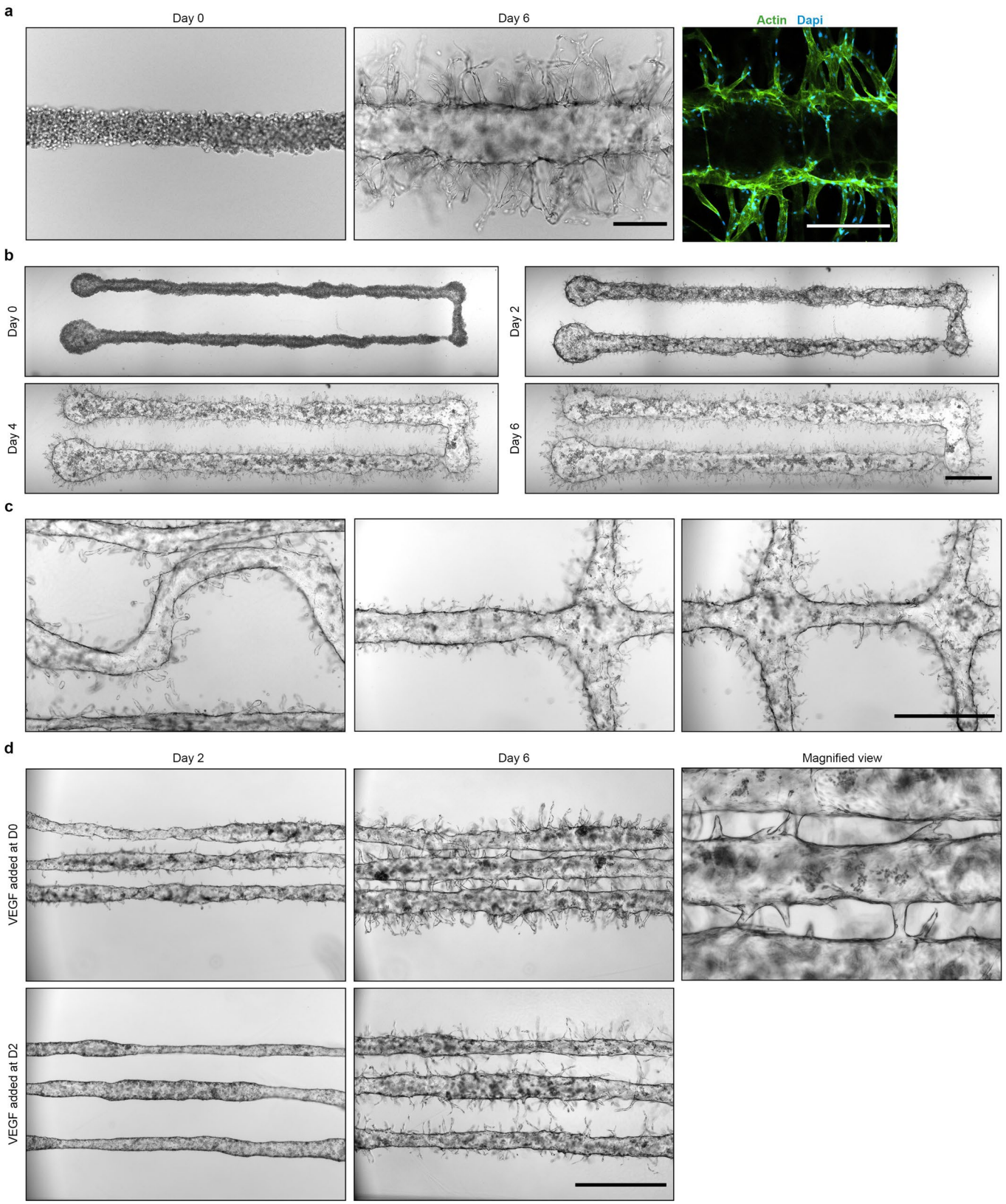

Extended Data Fig. 5 | Induction of angiogenesis in bioprinted vascular tubes. a, Evolution of a printed vascular tube exposed to high VEGF concentration. Many capillaries are formed *de novo* while maintaining the continuous lumen. Scale bars, 250 μm. **b**, Evolution of a printout with straight angles showing good conservation of the printing geometry over time. Scale bar, 1000 μm. **c**, Complex geometries can also be printed, resulting in branched vascular networks with strong angiogenesis potential. Scale bar, 1000 μm. **d**, Bright-field images showing the evolution of printed vascular tube with addition of VEGF at different time points. Angiogenesis can be triggered at a desired time, promoting formation of capillaries that can connect with other tubes. Images are representative of n = 3 biologically independent experiments. Scale bar, 1000 μm.

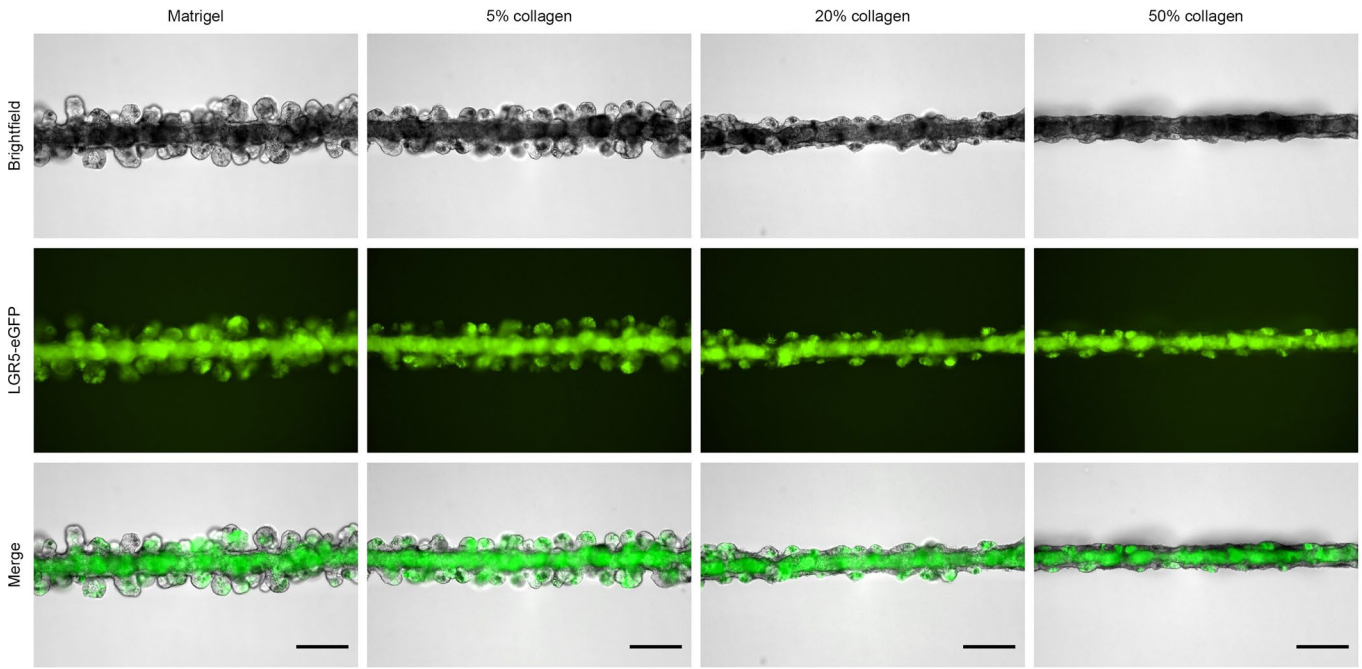

Extended Data Fig. 6 | Intestinal tube morphogenesis: influence of collagen content in the support hydrogel. Addition of collagen I increases the stiffness of the support hydrogel, limiting extensive budding of the tubes. Of note: when the gel is disrupted, budding can occur even at later time points also for initially stiffer hydrogels. Images are representative of n = 3 biologically independent experiments. Scale bars, 200 μm.

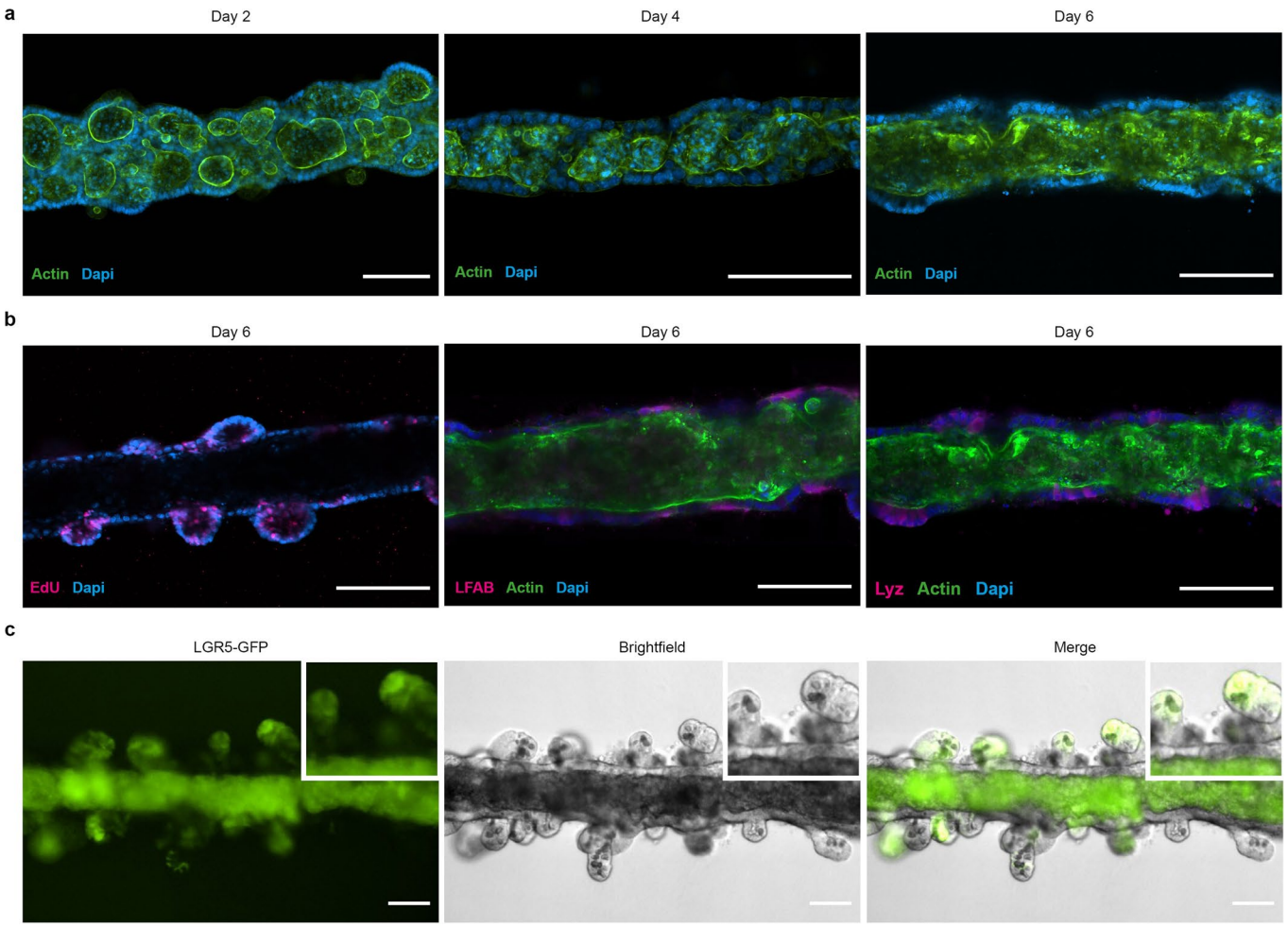

Extended Data Fig. 7 | Intestinal epithelial tube staining. a, Confocal fluorescent images showing the formation of a continuous lumen by colony fusion. Images are representative of n = 3 biologically independent experiments. Scale bars, 100 μm. **b**, Staining of the intestinal tubes after six days of culture. Proliferation (EdU, left) and Paneth cells (Lyz, right) are restricted to the crypt-like structures whereas enterocytes (LFAB, middle) are found on flatter surfaces. Images are representative of n = 3 biologically independent experiments. Scale bars, 100 μm. **c**, fluorescent image of LGR5-eGFP and corresponding bright-field image of a tube after seven days, showing darker Paneth cells intercalated in between stem cells inside the crypts. Note that the autofluorescence of dead cells in the lumen does not overlap with the intact epithelium in the merged picture. Images are representative of n = 3 biologically independent experiments. Scale bars, 100 μm.

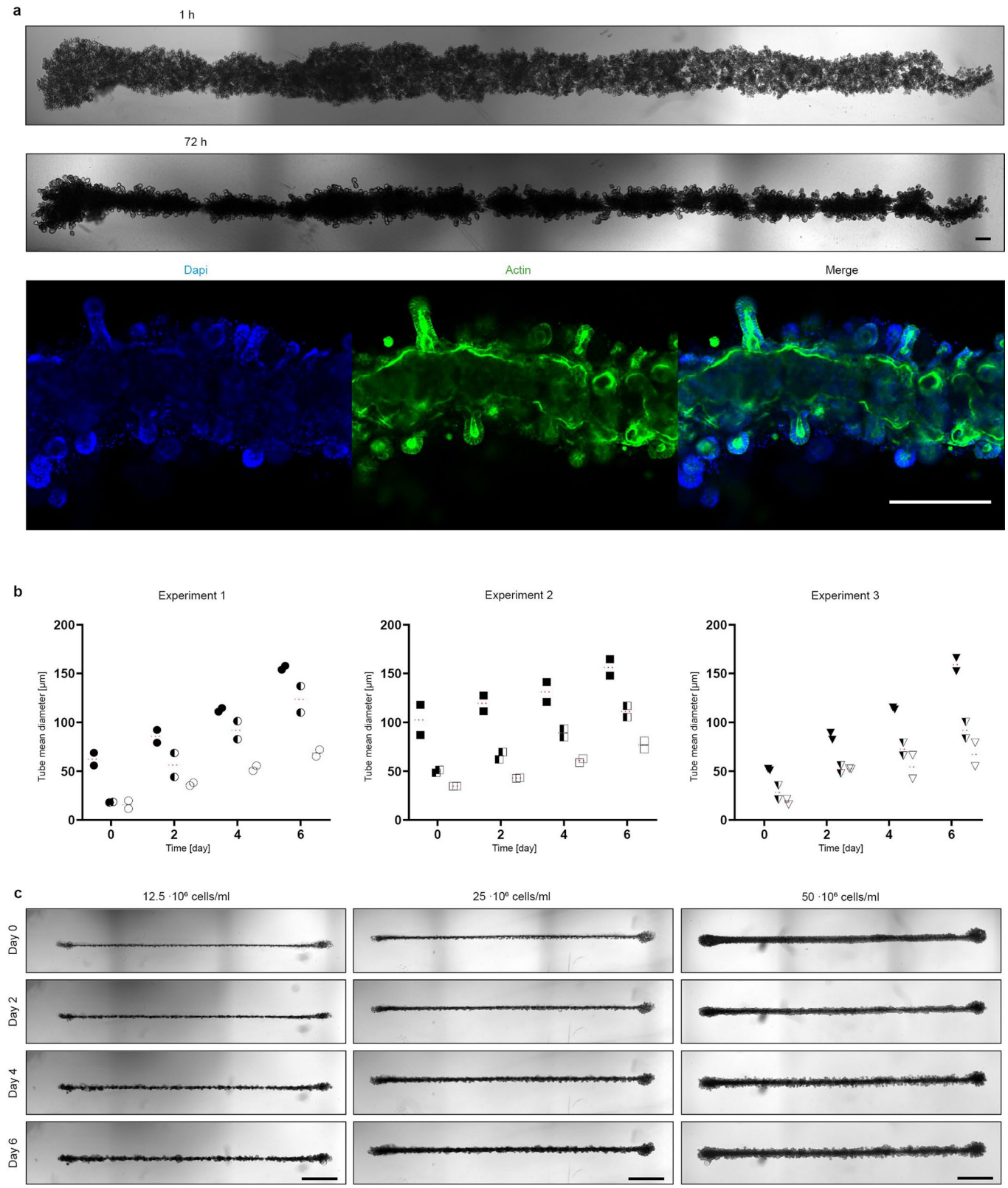

Extended Data Fig. 8 | Influence of printing cell density on tube formation and diameter. a, Representative tube printed from small intestinal organoids (*that is* not single cells). Top: 1 hour after printing, Middle: 72h after printing, Bottom: staining (Dapi labelling the nuclei, Actin) of the tube showing a lumen and crypt structures. Scale bars, 200 µm. **b**, Change of mean tube diameter over time at three different cell densities: 12,5 million (white symbol), 25 million (white and black symbol) and 50 million (black symbol) cells/ml. The experiment was repeated three times and two tubes are shown for each cell density. **c**, Evolution over time of one representative tube for each initial cell density from one of the three experiment is shown. Scale bars, 1000 µm.

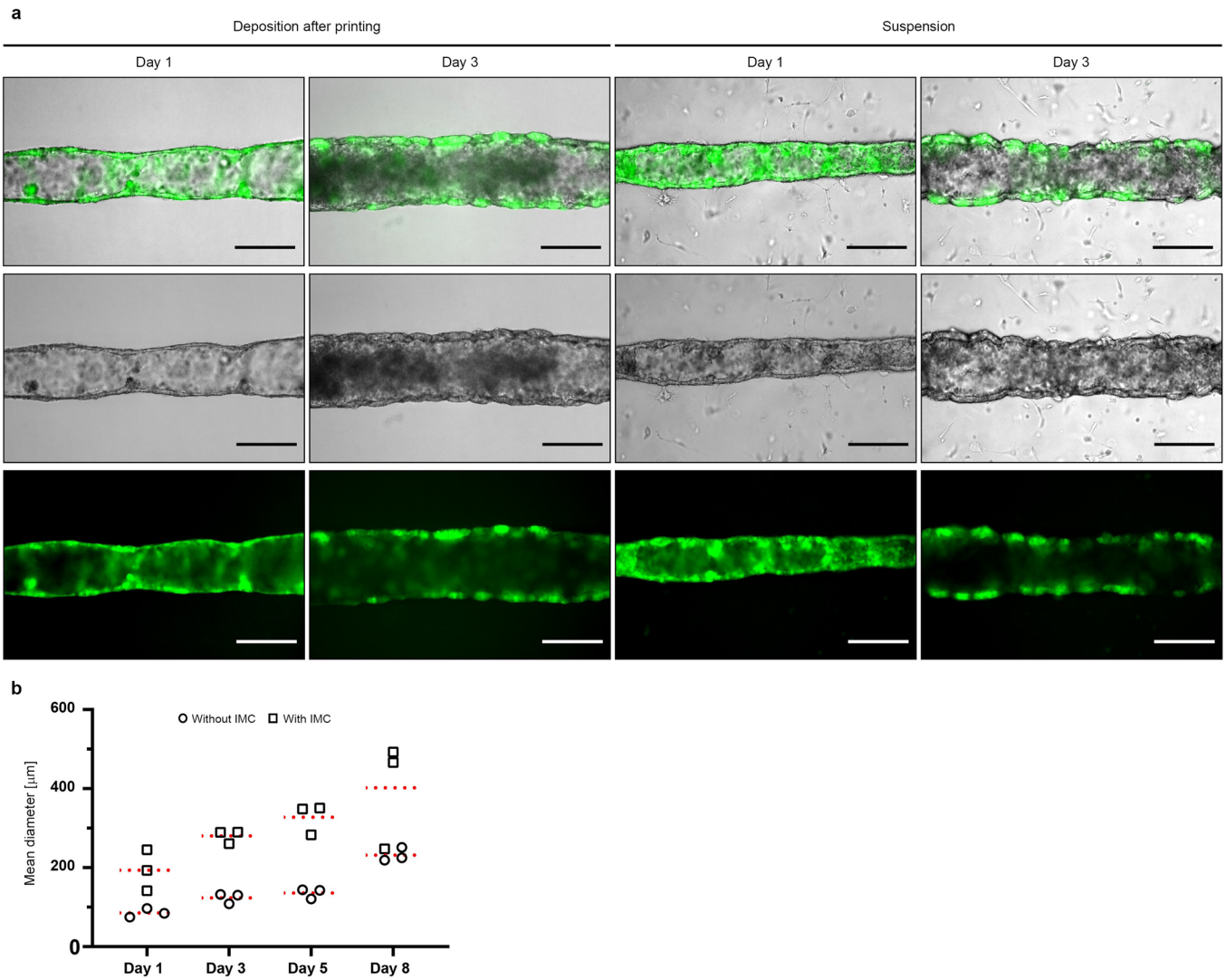

Extended Data Fig. 9 | Effect of IMC co-culture in bioprinted intestinal tubes. a, Bright-field images and corresponding fluorescent images of Lgr5-eGFP three days after printing, showing the effect of IMC co-culture on tube formation. IMCs were either deposited after printing for adherence on the well bottom and hydrogel (left), or directly suspended inside the hydrogel before and during printing (right). In all cases, a continuous lumen was formed after only one day, and the tubes comprise many Lgr5+ buds after 3 days. Images are representative of n = 3 biologically independent experiments. Scale bars, 250 µm. **b**, Difference in evolution of the tube diameter if co-cultured with IMCs or not. For each day, the mean diameter (dotted line) of tubes with and without myofibroblasts were compared (n=3 tubes for each day).

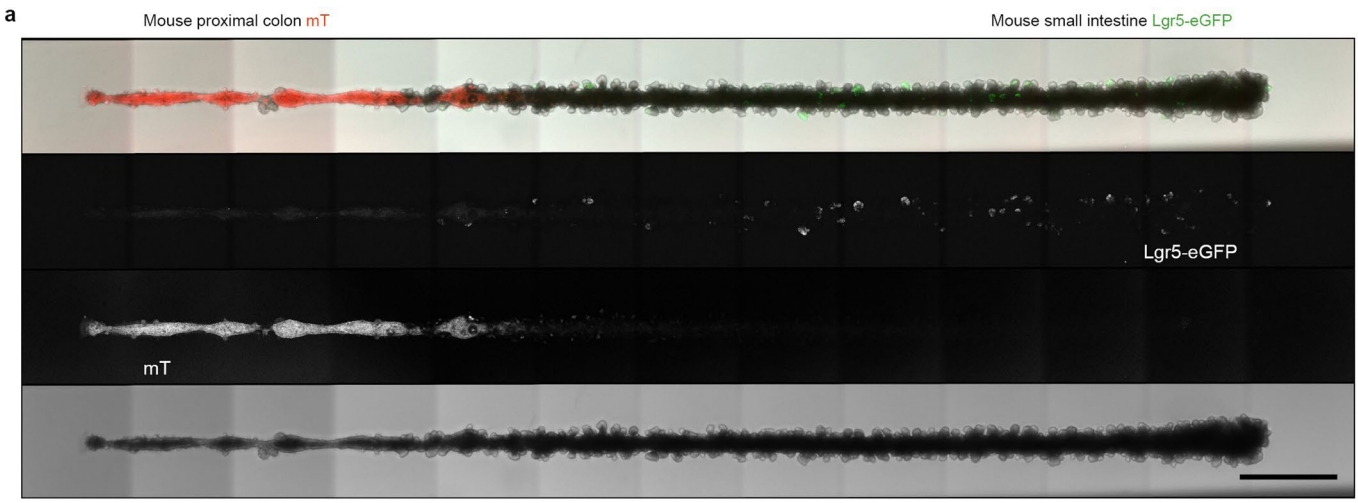

Extended Data Fig. 10 | Continuous epithelial tube composed of mouse small intestine and colon stem cells. Top: merged (max Z projection) image of the tube in bright-field as well as showing red (mT) and green (Lgr5-eGFP) fluorescent cells, each color being shown separately below. Middle: colon cells expressing mT and intestinal cells expressing Lgr5-eGFP. Bottom: bright-field. Images are representative of n = 3 biologically independent experiments. Scale bar, 1000 μm.

nature research

Corresponding author(s): Matthias P. Lutolf

Last updated by author(s): 2020/07/24

Reporting Summary

Nature Research wishes to improve the reproducibility of the work that we publish. This form provides structure for consistency and transparency in reporting. For further information on Nature Research policies, see Authors & Referees and the Editorial Policy Checklist.

Statistics

For all statistical analyses, confirm that the following items are present in the figure legend, table legend, main text, or Methods section.

n/a	Confirmed
☐	☒ The exact sample size (*n*) for each experimental group/condition, given as a discrete number and unit of measurement
☐	☒ A statement on whether measurements were taken from distinct samples or whether the same sample was measured repeatedly
☐	☒ The statistical test(s) used AND whether they are one- or two-sided *Only common tests should be described solely by name; describe more complex techniques in the Methods section.*
☒	☐ A description of all covariates tested
☐	☒ A description of any assumptions or corrections, such as tests of normality and adjustment for multiple comparisons
☐	☒ A full description of the statistical parameters including central tendency (e.g. means) or other basic estimates (e.g. regression coefficient) AND variation (e.g. standard deviation) or associated estimates of uncertainty (e.g. confidence intervals)
☐	☒ For null hypothesis testing, the test statistic (e.g. *F*, *t*, *r*) with confidence intervals, effect sizes, degrees of freedom and *P* value noted *Give P values as exact values whenever suitable.*
☒	☐ For Bayesian analysis, information on the choice of priors and Markov chain Monte Carlo settings
☒	☐ For hierarchical and complex designs, identification of the appropriate level for tests and full reporting of outcomes
☒	☐ Estimates of effect sizes (e.g. Cohen's *d*, Pearson's *r*), indicating how they were calculated

Our web collection on statistics for biologists contains articles on many of the points above.

Software and code

Policy information about availability of computer code

Data collection	Custom software was developed in LabView 2019 to control the printing process and liquid dispensing. ZEN 2010B SP1 (Zeiss) was used to acquire images from Zeiss LSM700 Confocal microscope. NIS-Elements 5.11 (Nikon) was used to acquire images from Nikon Eclipse Ti inverted microscope equipped with DS-Qi2 (brightfield) and Andor iXon Ultra cameras. LAS-X was used to acquire images from Leica SP8 microscope.
Data analysis	Image processing was performed using Fiji-ImageJ (v 2.0.0-rc-69/1.52i) and custom plugins for time-lapse image processing from Bioimaging Core Facility (BIOP, EPFL). Statistical analysis were performed using GraphPad Prism (8.2.0). QPCR data were visualized using QuantStudio Real-Time PCR Software (v1.3, Applied Biosystems). Adobe Illustrator CC 2019, Adobe Photoshop CC 2019 and Adobe Premiere Pro CC 2019 were used to design illustrations and supplementary movies rendering.

For manuscripts utilizing custom algorithms or software that are central to the research but not yet described in published literature, software must be made available to editors/reviewers. We strongly encourage code deposition in a community repository (e.g. GitHub). See the Nature Research guidelines for submitting code & software for further information.

Data

Policy information about availability of data

All manuscripts must include a data availability statement. This statement should provide the following information, where applicable:

- Accession codes, unique identifiers, or web links for publicly available datasets
- A list of figures that have associated raw data
- A description of any restrictions on data availability

The datasets supporting the conclusions of this article are included within the article and its additional files.

Field-specific reporting

Please select the one below that is the best fit for your research. If you are not sure, read the appropriate sections before making your selection.

☒ Life sciences ☐ Behavioural & social sciences ☐ Ecological, evolutionary & environmental sciences

For a reference copy of the document with all sections, see nature.com/documents/nr-reporting-summary-flat.pdf

Life sciences study design

All studies must disclose on these points even when the disclosure is negative.

Sample size	The study is aimed at the development of a novel bioprinting concept. No specific hypothesis was tested and no sample calculation, allocation of samples to different groups and randomization was performed. Multiple tissues (n>3) were printed for each experiments and representative images are shown for microscopy, histology, TEM and macroscopic views. For viability studies, 3 biologically independent experiments were performed for each cell type and condition. Length and diameter quantification shows the results of two tubes. Three different experiments were used to assess forskolin-induced swelling, with two treated and one control tubes in each experiment. Experiments on density were repeated three different times with each two tubes per condition. At least two tubes per conditions were averaged for gene expression results obtained by qPCR. Three tubes per condition were used for the experiment assessing the effect of myofibroblasts on tube diameter.
Data exclusions	No data acquired for quantitative analysis were excluded.
Replication	The vast majority of the conditions have been independently experimentally repeated a minimum of three times. In all the attempts at repetition for each specific condition we observed similar behavior concerning the spatiotemporal reorganization of the cells.
Randomization	Bioprinted tissues were randomly allocated into the experimental groups.
Blinding	Investigators were not blinded with respect to the identities of the samples. However, all experimental and control samples were collected/ analyzed at the same time under the same condition, and data analysis was carried out with the same software settings.

Reporting for specific materials, systems and methods

We require information from authors about some types of materials, experimental systems and methods used in many studies. Here, indicate whether each material, system or method listed is relevant to your study. If you are not sure if a list item applies to your research, read the appropriate section before selecting a response.

Materials & experimental systems

n/a	Involved in the study
☐	☒ Antibodies
☐	☒ Eukaryotic cell lines
☒	☐ Palaeontology
☐	☒ Animals and other organisms
☐	☒ Human research participants
☒	☐ Clinical data

Methods

n/a	Involved in the study
☒	☐ ChIP-seq
☒	☐ Flow cytometry
☒	☐ MRI-based neuroimaging

Antibodies

Antibodies used

Lysozyme (Thermo fisher scientific #PA1-29680, clone NA (Polyclonal), dilution 1:50)
Mucin2 (Santa Cruz #sc-15334, clone NA (Polyclonal), lot K0315 no longer available, dilution 1:50)
Chromogranin-A (Santa Cruz #sc-13090, clone NA (Polyclonal),no longer available, dilution 1:50)
L-FABP (Santa Cruz #sc-50380, clone NA (Polyclonal), dilution 1:50)
E-cadherin (Abcam #ab11512, clone DECMA-1, dilution 1:50)
Sox9 (Abcam #ab185966, clone EPR14335-78, dilution 1:50)
CD31 (1:200; Cell Signalling Tech #3528S),
alpha smooth muscle actin (1:100; DAKO/Agilient) #M0851),
DAPI (1:2000; ThermoFisher Scientific #D1306),
Alexa Fluor 647 goat anti rabbit IgG (Thermo fisher scientific A21245, clone NA (Polyclonal), dilution 1:500)
Alexa Fluor 546 goat anti mouse IgG (Thermo fisher scientific A11030, clone NA (Polyclonal), dilution 1:500)
Alexa Fluor 488 goat anti rat IgG (Thermo fisher scientific A11006, clone NA (Polyclonal), dilution 1:500)
Alexa Fluor 568 donkey anti mouse IgG (Thermo fisher scientific A10037, clone NA (Polyclonal), dilution 1:500)
Alexa Fluor 568 donkey anti rabbit IgG (Thermo fisher scientific A10042, clone NA (Polyclonal), dilution 1:1000)
Alexa Fluor 647 donkey anti mouse IgG (Thermo fisher scientific A-31571, clone NA (Polyclonal), dilution 1:1000
Alexa Fluor 647 donkey anti rabbit IgG (Thermo fisher scientific A31573, clone NA (Polyclonal), dilution 1:500)

Alexa Fluor 546 Phalloidin (Thermo fisher scientific A22283, dilution 1:40)
Alexa Fluor 488 Phalloidin (Thermo fisher scientific A12379, dilution 1:40)

Validation

In the immunofluorescence procedure a "No Primary Control sample" and an "Undifferentiated Control sample" were used as reference for background signal.
Validation statements available from manufacturers:
Lysozyme (https://www.thermofisher.com/antibody/product/Lysozyme-Antibody-Polyclonal/PA1-29680, additionally validated in ref: Designer matrices for intestinal stem cell and organoid culture)
Mucin2 (https://www.scbt.com/p/mucin-2-antibody-h-300, discontinued, additionally validated in ref: Single Lgr5 stem cells build crypt-villus structures in vitro without a mesenchymal niche)
Chromogranin-A (https://www.scbt.com/p/chr-a-antibody-h-300, discontinued, additionally validated in ref: Designer matrices for intestinal stem cell and organoid culture)
E-cadherin (https://www.abcam.com/e-cadherin-antibody-decma-1-intercellular-junction-marker-ab11512.html)
Sox9 (https://www.abcam.com/sox9-antibody-epr14335-78-ab185966.html)
L-FABP (https://www.scbt.com/p/l-fabp-antibody-h-120, discontinued, additionally validated in ref: Designer matrices for intestinal stem cell and organoid culture)
CD31 validated HUVECs (https://www.cellsignal.com/products/primary-antibodies/cd31-pecam-1-89c2-mouse-mab/3528), alpha smooth muscle actin validated on smooth muscle cells, myofibroblasts and myoepithelial cells(https://www.agilent.com/en/product/immunohistochemistry/antibodies-controls/primary-antibodies/actin-(smooth-muscle)-(concentrate)-76542).
Alexa Fluor 647 goat anti rabbit IgG (https://www.thermofisher.com/antibody/product/Goat-anti-Rabbit-IgG-H-L-Highly-Cross-Adsorbed-Secondary-Antibody-Polyclonal/A-21245)
Alexa Fluor 546 goat anti mouse IgG (https://www.thermofisher.com/antibody/product/Goat-anti-Mouse-IgG-H-L-Highly-Cross-Adsorbed-Secondary-Antibody-Polyclonal/A-11030)
Alexa Fluor 488 goat anti rat IgG (https://www.thermofisher.com/antibody/product/Goat-anti-Rat-IgG-H-L-Cross-Adsorbed-Secondary-Antibody-Polyclonal/A-11006)
Alexa Fluor 568 donkey anti mouse IgG (https://www.thermofisher.com/antibody/product/Donkey-anti-Mouse-IgG-H-L-Highly-Cross-Adsorbed-Secondary-Antibody-Polyclonal/A10037)
Alexa Fluor 647 donkey anti rabbit IgG (https://www.thermofisher.com/antibody/product/Donkey-anti-Rabbit-IgG-H-L-Highly-Cross-Adsorbed-Secondary-Antibody-Polyclonal/A-31573)
Alexa Fluor 546 Phalloidin (https://www.thermofisher.com/order/catalog/product/A22283)
Alexa Fluor 488 Phalloidin (https://www.thermofisher.com/order/catalog/product/A12379)

Eukaryotic cell lines

Policy information about cell lines

Cell line source(s)

C2C12 were obtained from ATCC. Human MSCs and HUVECs were obtained from Lonza.
Intestinal crypts (intestinal stem cells) were isolated from 6–13-week-old heterozygous Lgr5–eGFP-IRES-CreERT2 (Jackson Laboratory), pLysDsRed (gift from Clevers lab) or wild-type C57BL/6 mice. Colon crypts (stem cells) were isolated from 6–13-week-old C57BL/6 mice or mTmG mouse (Jackson Laboratory). Stomach glands were isolated from 6–13-week-old mTmG mouse (Jackson Laboratory). Intestinal mesenchymal cells (IMC) were isolated from 6–13-week-old C57BL/6 mice.
Human small intestinal organoids were kindly provided by Hans Clevers lab (Hubrecht Institute) within the framework of collaboration agreement, OSR-2020-027B. Endoscopic biopsies were performed at the University Medical Center Utrecht and the Wilhelmina Children's Hospital. The patients' informed consent was obtained, and this study was approved by the ethical committee of the University Medical Center Utrecht.
Cell lines used to produce Noggin, R-spondin and Wnt conditioned medium were acquired from Hubrecht Institute, (Uppsalalaan B,3584 CT Utrecht, The Netherlands), medium was produced according to a previously published protocol.
Triple Wnt/R-Spondin/Noggin (WRN)-conditioned medium was produced using L-WRN cells (ATCC, CRL-3276) according to a previously published protocol.

Authentication

C2C12, HUVEC and MSC were authenticated at the time of purchase.

Mycoplasma contamination

All the cell lines used in this work have been routinely tested for mycoplasma infection and they resulted negative.

Commonly misidentified lines
(See ICLAC register)

The cell lines used in this study are NOT present in the ICLAC register.

Animals and other organisms

Policy information about studies involving animals; ARRIVE guidelines recommended for reporting animal research

Laboratory animals

Intestinal crypts (intestinal stem cells) were isolated from 6–13-week-old heterozygous Lgr5–eGFP-IRES-CreERT2 (Jackson Laboratory), pLysDsRed (gift from Clevers lab) or wild-type C57BL/6 mice. Colon crypts (stem cells) were isolated from 6–13-week-old C57BL/6 mice or mTmG mouse (Jackson Laboratory). Stomach glands were isolated from 6–13-week-old mTmG mouse (Jackson Laboratory). Intestinal mesenchymal cells (IMC) were isolated from 6–13-week-old C57BL/6 mice.

Wild animals

The study did not involve wild animals

Field-collected samples

The study did not involve samples collected from the field

Ethics oversight

All animal experiments were approved by the Vaud Cantonal Veterinary Authorities and conducted in compliance with the animal experimentation protocols prescribed by EPFL and FELASA, local animal welfare laws and guidelines.

Note that full information on the approval of the study protocol must also be provided in the manuscript.

Human research participants

Policy information about studies involving human research participants

Population characteristics	Endoscopic biopsies were performed at the University Medical Center Utrecht and the Wilhelmina Children's Hospital. We did not interact or select human patients.
Recruitment	This study didn't involve patients recruitment.
Ethics oversight	Endoscopic biopsies were performed at the University Medical Center Utrecht and the Wilhelmina Children's Hospital. The patients' informed consent was obtained, and this study was approved by the ethical committee of the University Medical Center Utrecht.

Note that full information on the approval of the study protocol must also be provided in the manuscript.